Suppression of mesoscale eddy mixing by topographic PV gradients

Miriam Frauke Sterl[1,2], Joseph H Lacasce[3], Sjoerd Groeskamp[1], Aleksi Nummelin[4,5], Pål E Isachsen[3,6], and Michiel L J Baatsen[2]

[1]NIOZ Royal Netherlands Institute for Sea Research
[2]Institute for Marine and Atmospheric Research, Utrecht University
[3]Department of Geosciences, University of Oslo
[4]NORCE Norwegian Research Centre AS
[5]Finnish Meteorological Institute
[6]Norwegian Meteorological Institute

March 07, 2024

Suppression of mesoscale eddy mixing by topographic PV gradients

Miriam F. Sterl,[a,b] Joseph H. LaCasce,[c] Sjoerd Groeskamp,[a] Aleksi Nummelin,[d,e] Pål E. Isachsen,[c,f] Michiel L. J. Baatsen[b]

[a] *NIOZ Royal Netherlands Institute for Sea Research, Texel, The Netherlands*

[b] *Institute for Marine and Atmospheric Research, Utrecht University, Utrecht, The Netherlands*

[c] *Department of Geosciences, University of Oslo, Oslo, Norway*

[d] *NORCE Norwegian Research Centre AS, Bergen, Norway*

[e] *Finnish Meteorological Institute, Helsinki, Finland*

[f] *Norwegian Meteorological Institute, Oslo, Norway*

Corresponding author: Miriam F. Sterl, miriam.sterl@nioz.nl

ABSTRACT: Oceanic mesoscale eddy mixing plays a crucial role in the Earth's climate system by redistributing heat, salt and carbon. For many ocean and climate models, mesoscale eddies still need to be parameterized. This is often done via an eddy diffusivity, $\mathcal{K}$, which sets the strength of turbulent downgradient tracer fluxes. A well known effect is the modulation of $\mathcal{K}$ in the presence of background potential vorticity (PV) gradients, which suppresses cross-PV gradient mixing. Topographic slopes can induce such suppression through topographic PV gradients. However, this effect has received little attention, and topographic effects are often not included in parameterizations for $\mathcal{K}$. In this study, we show that it is possible to describe the effect of topography on $\mathcal{K}$ analytically in a barotropic framework, using a simple stochastic representation of eddy-eddy interactions. We obtain an analytical expression for the depth-averaged $\mathcal{K}$ as a function of the bottom slope, which we validate against diagnosed eddy diffusivities from a numerical model. The obtained analytical expression can be generalized to any constant barotropic PV gradient. Moreover, the expression is consistent with empirical parameterizations for eddy diffusivity over topography from previous studies and provides a physical rationalization for these parameterizations. The new expression helps to understand how eddy diffusivities vary across the ocean, and thus how mesoscale eddies impact ocean mixing processes.

SIGNIFICANCE STATEMENT: Large oceanic 'whirls', called eddies, can mix and transport ocean properties such as heat, salt, carbon and nutrients. Mixing plays an important role for oceanic ecosystems and the climate system. In numerical simulations of the Earth's climate, eddy mixing is typically represented using a simplified expression. However, an effect that is often not included is that eddy mixing is weaker over a sloping seafloor. In most areas of the ocean the bottom slope is steep enough for this effect to be significant. In this study we derive an expression for eddy mixing that accounts for oceanic bottom slopes. The present effort provides a physical basis for eddy mixing over oceanic bottom slopes, justifying their use in climate models.

1. Introduction

Oceanic mesoscale eddies play a key role in the global ocean circulation, oceanic ecosystems and the climate system as a whole. Eddies mix, transport, and store tracers such as heat, salt, carbon, oxygen, and nutrients (Lee et al. 2007; Gruber et al. 2011; Gnanadesikan et al. 2013, 2015, 2017; Stewart et al. 2018; Busecke and Abernathey 2019; Jones and Abernathey 2019; Groeskamp et al. 2019). However, mesoscale eddies occur on spatial scales of 10–100 km, which is in the same order or smaller than the horizontal grid resolution of most global climate models (Eden 2007; Chelton et al. 2011; Hallberg 2013; LaCasce and Groeskamp 2020; Martínez-Moreno et al. 2022). Therefore, mesoscale mixing processes are often not explicitly resolved in climate simulations, and instead need to be parameterized (Eden and Greatbatch 2008; Hallberg 2013; Jansen et al. 2015; Zanna et al. 2017; Fox-Kemper et al. 2019; Wang and Stewart 2020). Parameterization of eddy mixing is typically done via an eddy diffusivity, $\mathcal{K}$, which relates the turbulent downgradient flux of a tracer $\mathcal{F}_C$ to the mean lateral tracer gradient ∇C as $\mathcal{F}_C = -\mathcal{K}\nabla C$. A distinction can be made between buoyancy diffusivity, which describes an eddy induced advection that resembles a diffusion of buoyancy (Gent and McWilliams 1990; Gent et al. 1995; McDougall and McIntosh 2001), and isopycnal diffusivity representing eddy diffusive fluxes that mix tracers along isopycnals (Redi 1982; Griffies 1998).

Significantly, climate models are very sensitive to the choice of the diffusivity value (e.g. Ferreira et al. 2005; Pradal and Gnanadesikan 2014; Gnanadesikan et al. 2015; Kjellsson and Zanna 2017; Jones and Abernathey 2019; Holmes et al. 2022; Mak et al. 2022b). In simulations of the Earth's climate, an approximately five-fold increase in the value of $\mathcal{K}$ can result in differences of 1°C in

the global-mean surface air and sea surface temperatures (Pradal and Gnanadesikan 2014), 20% variation in anthropogenic carbon uptake (Gnanadesikan et al. 2015), and a decrease in the residual meridional overturning circulation in the North Atlantic and the Antarctic Circumpolar Current volume transport in the Southern Ocean by around 30% (Chouksey et al. 2022). It is thus of great importance to know how to accurately parameterize $\mathcal{K}$ in global climate models.

Many paramaterizations of $\mathcal{K}$ are based on mixing length theory (Prandtl 1925), which suggests a scaling of the form $K \sim \mathcal{V}\mathcal{L}$, where $\mathcal{V}$ is the root mean squared eddy velocity and $\mathcal{L}$ is a mixing length. The mixing length can be thought of as a length scale over which the eddy field can effectively mix tracers. Mixing length theory was applied to create the first global estimates of eddy diffusivity at the sea surface (Holloway 1986; Keffer and Holloway 1988; Stammer 1998).

Holloway and Kristmannsson (1984) and Holloway (1986) suggested that if eddies have Rossby wave characteristics, the eddy diffusivity is suppressed. This suppression effect was later shown analytically by e.g. Ferrari and Nikurashin (2010) (using a passive tracer approach), Klocker et al. (2012) (using a Lagrangian approach), and Griesel et al. (2015) (using linear stability analysis). In all of these studies, eddy fields are represented as statistically forced and linearly damped Rossby waves, and it is shown that the cross-stream mixing length is effectively reduced in the presence of a background mean flow if the eddies are propagating relative to the mean flow.

A kinematic interpretation of the suppression mechanism is that the mean flow will advect tracers through the eddy field before the eddy field has had time to mix the tracers in the cross-stream direction. If the eddies did not have an intrinsic phase speed, they would move with the mean flow and thus be able to effectively mix the tracers. The parameterization of Ferrari and Nikurashin (2010) has been widely used in idealized models (Nakamura and Zhu 2010b; Eden 2011; Srinivasan and Young 2014; Kong and Jansen 2017; Wolfram and Ringler 2017; Seland et al. 2020) and validated and applied to the Antarctic Circumpolar Current (Naveira Garabato et al. 2011; Sallée et al. 2011; Meredith et al. 2012; Pennel and Kamenkovich 2014; Chen et al. 2015; Roach et al. 2016; Chapman and Sallée 2017), the Kuroshio Extension (Chen et al. 2014), the Gulf Stream (Bolton et al. 2019), the Nordic Seas (Isachsen and Nøst 2012), eastern boundary currents (Bire and Wolfe 2018), and the global ocean (Bates et al. 2014; Klocker and Abernathey 2014; Roach et al. 2018; Busecke and Abernathey 2019; Canuto et al. 2019; Groeskamp et al. 2020).

A different interpretation from the kinematic explanation described above is that the suppression is a dynamical effect caused by gradients in potential vorticity (PV). Marshall et al. (2006) estimated surface eddy diffusivities in the Southern Ocean from satellite altimetry, and found that regions of high and low diffusivity coincide with regions of weak and strong PV gradients, respectively. They suggested that strong PV gradients impose a barrier on lateral transport, inhibiting cross-stream diffusivity. This effect is also observed in the atmosphere (e.g. Dritschel and McIntyre 2008). Nakamura and Zhu (2010b), Klocker et al. (2012), Srinivasan and Young (2014) and Balwada et al. (2016) explicitly linked the mixing barriers caused by PV gradients to the parameterization of Ferrari and Nikurashin (2010) by noting that the PV gradient determines the Rossby wave phase speed; hence, it is the PV gradient that enables the eddies to move relative to the mean flow, which leads to the suppression of the cross-stream eddy diffusivity.

Previous studies have mainly focused on PV gradients caused by the planetary β-effect (latitudinal variations of the Coriolis parameter). However, an important factor that should also be considered is the effect of topography. If it is indeed the PV gradient that causes the suppression effect, then we must consider the role of topography as well, because topographic slopes contribute significantly to (barotropic) PV gradients (LaCasce and Speer 1999; LaCasce 2000) and permit topographic Rossby waves (Rhines 1970; Csanady 1976; Hogg 2000). Hence, topographic slopes can also be expected to modulate eddy diffusivity (Jansen et al. 2015). Isachsen (2011) diagnosed eddy diffusivities for different bottom slopes from numerical simulations, and found that the diffusivities were highest for flat bottoms, suggesting a suppression effect of topographic slopes. A relevant question then is how exactly does topography modulate eddy diffusivities, and how to parameterize topographic effects related to eddy mixing. Since topography steers currents, its effects might already be included in the mean flow term from Ferrari and Nikurashin (2010), but only implicitly.

Some recent studies have aimed to express the eddy diffusivity explicitly in terms of topographic slopes using numerical model data. Diagnostic expressions were derived from high-resolution simulations by Brink (2012), Brink and Cherian (2013) and Brink (2016), by Wang and Stewart (2020) and Wei et al. (2022) for buoyancy diffusivity specifically, and by Wei and Wang (2021) for isopycnal diffusivity specifically. Moreover, Nummelin and Isachsen (2024) and Wei et al. (2024) derived parameterizations for the buoyancy diffusivity over topographic slopes and tested them in prognostic coarse-resolution simulations. All of these studies derived parameterizations

for the eddy diffusivities using various scaling estimates for the mixing length combined with empirical 'suppression' functions. Although the suppression functions from the aforementioned studies perform well in representing suppression of eddy diffusivity by topographic slopes, they are essentially empirical fits to functions that have little dynamical justification. Therefore, the aim of this study is to derive an analytical expression for the suppression of $\mathcal{K}$ that is dynamically linked to the topographic PV gradient. Such an expression can provide insight into the physical mechanisms through which topography suppresses eddy diffusivities. On a practical level, it can also help in making more accurate estimates of eddy diffusivities across the world's oceans. The focus of this work is on the suppression effect of topography, without particularly focusing on buoyancy or isopycnal diffusivity. Diagnosing diffusivity will be done with downgradient fluxes of both buoyancy and PV.

The rest of this article is organized as follows. In section 2, we derive the analytical model. In section 3, we compare the analytical expression for $\mathcal{K}$ with diagnosed diffusivities from a numerical model. Section 4 discusses the theoretical and numerical results. Finally, a summary and conclusion are given in section 5.

2. Theory

The starting point is the Quasi-Geostrophic Potential Vorticity (QGPV) equation. As we are interested in the effects of topographic PV, we work with the barotropic QGPV equation, which explicitly includes a topographic PV term. The barotropic and rigid lid QGPV equation on a β-plane, in the absence of forcing and dissipation, says that the QGPV, q [s^{-1}], is materially conserved (e.g. Dijkstra 2008):

$$\frac{d_g}{dt} q = 0, \quad q = \underbrace{\nabla^2 \psi}_{\text{relative vorticity}} + \underbrace{\beta_0 y}_{\text{planetary PV}} + \underbrace{\frac{f_0}{H} h_b}_{\text{topographic PV}} . \tag{1}$$

Here $\frac{d_g}{dt} = \partial_t + u_g \partial_x + v_g \partial_y$, where u_g and v_g [m s^{-1}] are the zonal and meridional geostrophic velocities, which are related to the geostrophic streamfunction ψ [m^2 s^{-1}] as $(u_g, v_g) = (-\partial\psi/\partial y, \partial\psi/\partial x)$. Furthermore, f_0 [s^{-1}] is the Coriolis parameter at some fixed latitude φ_0 and β_0 [m^{-1} s^{-1}] is the meridional gradient of the Coriolis parameter at φ_0; both f_0 and β_0 are assumed constant here

(β-plane approximation). The meridional coordinate relative to φ_0 is denoted by y [m]. Finally, H [m] is the mean water depth, while $h_b = h_b(x, y)$ [m] is the topographic variation superimposed on H, with $|h_b| \ll H$.

We decompose ψ, q and $\mathbf{u_g}$ into time-mean components (denoted by $\Psi, Q, \mathbf{U}$) and eddy components (denoted by $\psi', q', \mathbf{u}'$). The velocities and streamfunctions are related to each other as $\mathbf{U} = (-\partial\Psi/\partial y, \partial\Psi/\partial x)$ and $\mathbf{u}' = (-\partial\psi'/\partial y, \partial\psi'/\partial x)$. We assume that the mean flow varies on spatial scales much larger than the eddy field; hence, it is approximately constant in both space and time. Then the mean relative vorticity $\nabla^2\Psi = 0$, so that the mean PV is determined by the planetary PV and topographic PV. Additionally, we assume that the mean flow $\mathbf{U}$ is parallel to mean PV contours (Pedlosky 1987; Vallis and Maltrud 1993), so that $\mathbf{U} \cdot \nabla Q = 0$. We then rotate the coordinate system such that the x-direction is aligned with the direction of the mean PV contours. Hence, the mean flow can be expressed as $\mathbf{U} = (U, 0)$; furthermore, the mean PV gradient is $\nabla Q = (0, \partial Q/\partial y)$, which we assume to be constant. With these assumptions the QGPV equation can be rewritten as

$$\frac{\partial q'}{\partial t} + \mathbf{U} \cdot \nabla q' + \mathbf{u}' \cdot \nabla Q = \mathcal{N}, \tag{2}$$

where $\mathcal{N}$ denotes the nonlinear terms $\mathbf{u}' \cdot \nabla q'$, interpreted as eddy-eddy interactions. Note that equation (2) is Galilean invariant.

From here, the derivation is analogous to that of Klocker et al. (2012), and we only discuss the key steps below; details of the derivation can be found in Appendix A. We express the eddy streamfunction ψ' as a monochromatic Rossby wave, given by

$$\psi'(x, y, t) = \mathrm{Re}\left(a(t) e^{ikx + ily}\right), \tag{3}$$

where k and l are the zonal and meridional wavenumbers, respectively. Substituting (3) into (2) and using (1) to relate q' to ψ', we obtain an ordinary differential equation for the wave amplitude $a(t)$, given by:

$$\frac{da}{dt} + ikc_w a = \mathcal{N}. \tag{4}$$

Here c_w is the total eddy phase speed relative to the ground (or eddy drift speed), which can be written as:

$$c_w = U + c, \quad c = -\frac{\partial Q/\partial y}{\kappa^2}, \tag{5}$$

where $\kappa \equiv \sqrt{k^2 + l^2}$ is the wavenumber magnitude and c is the intrinsic Rossby wave phase speed relative to the mean flow, given by the dispersion relation for Rossby waves (e.g. Dijkstra 2008). To obtain analytical solutions to (4), we assume the nonlinear eddy-eddy interactions have a fluctuation-dissipation stochastic representation (DelSole 2004; Ferrari and Nikurashin 2010; Klocker et al. 2012), given by

$$\mathcal{N} = Ar(t) - \gamma a(t). \tag{6}$$

Here, $r(t)$ is a white noise random process with A setting its amplitude. Energy dissipates through linear damping, and γ is the damping rate or inverse eddy decorrelation timescale. It is called a 'decorrelation' timescale because the cross-stream eddy velocity autocovariance decays exponentially in time with γ^{-1} the e-folding timescale (equation A14 in Appendix A). Combining (4) and (6) and expressing the eddy kinetic energy (EKE), $\mathcal{U}^2/2$, in terms of the eddy velocities as

$$\mathcal{U}^2 = \langle u'^2 \rangle + \langle v'^2 \rangle, \tag{7}$$

it is possible to find an analytical solution for $a(t)$ (see equations A1–A7 in Appendix A). Given $a(t)$, we can get an expression for the eddy streamfunction $\psi'(x, y, t)$ (equation A8), which then gives us expressions for the eddy flow velocities. From knowledge of the eddy flow velocities, we can then compute eddy diffusivities. We will focus on the diffusivity in the cross-stream direction (here: y) because in the along-stream direction advection by the mean flow is dominant over eddy diffusion (LaCasce et al. 2014). We compute the eddy diffusivity as the Taylor diffusivity (Taylor 1921), which applies to passive tracer particles and is defined as the derivative of the mean squared separation of particles from their starting position. The Taylor diffusivity can also be written as the autocorrelation of the Lagrangian cross-stream eddy velocity (Taylor 1921; Davis 1987, 1991;

LaCasce 2008; LaCasce et al. 2014):

$$\mathcal{K} = \lim_{t\to\infty} \frac{1}{2}\frac{d}{dt}\eta^2 = \lim_{t\to\infty} \mathrm{Re}\left(\int_0^t \left\langle v_L(t) v_L^*(t')\right\rangle \mathrm{d}t'\right), \tag{8}$$

where η is the particle displacement and $v_L = v_L(t;x,y,0)$ is the Lagrangian velocity of a particle at time t that was at (x,y) at $t=0$. We approximate $v_L(t;x,y,0)$ with the Eulerian velocity for a particle advected by the mean flow, $v'(x+Ut,y,t)$, for which we can get an analytical expression via the streamfunction relation $v' = -\partial\psi'/\partial x$. This finally gives us the following expression for the cross-stream eddy diffusivity (see equations A9–A17 in Appendix A):

$$\mathcal{K} = \frac{\mathcal{K}_0}{1+\frac{k^2}{\gamma^2}(c_w - U)^2} \equiv \mathcal{S}\mathcal{K}_0, \tag{9}$$

with

$$\mathcal{K}_0 \equiv \frac{\mathcal{A}\mathcal{U}^2}{\gamma}. \tag{10}$$

Here, $\mathcal{A} = k^2/\kappa^2$ is the eddy anisotropy factor (Wei and Wang 2021), representing the magnitude of the along-stream wavenumber relative to the total wavenumber magnitude. The factor $\mathcal{S}$ is the 'suppression factor', and $\mathcal{K}_0$ is the unsuppressed diffusivity. Note that $\mathcal{K}_0$ follows a mixing length scaling (Prandtl 1925) where the mixing length is set by $\mathcal{L} = \mathcal{U}/\gamma$, i.e. the mixing length depends on the EKE. As noted by Ferrari and Nikurashin (2010), from (9) it can be seen that the eddy diffusivity is suppressed if $c_w - U \neq 0$, i.e. if the eddies have an intrinsic phase speed and are moving relative to the mean flow. Suppression is strong when $k(c_w - U) \gg \gamma$, i.e. when the advection timescale is shorter than the eddy decorrelation timescale. On the other hand, if the eddy field decorrelates faster than the advective timescale, i.e. $k(c_w - U) \ll \gamma$, the suppression effect is negligible. Equation (9) is equivalent to equation (14) of Ferrari and Nikurashin (2010) and equation (20) of Klocker et al. (2012), and has been applied in many studies. Note that (9) is a general expression that applies to any form of the barotropic QGPV equation (1) assuming a constant PV gradient.

One can also express $\mathcal{K}$ in terms of the PV gradient by using equation (5) to replace the mean flow term $c_w - U$ in (9) by c, the intrinsic eddy phase speed. The intrinsic phase speed is determined by

the PV gradient via the dispersion relation for Rossby waves:

$$|c| = \frac{|\nabla Q|}{\kappa^2}. \tag{11}$$

Substituting (11) and the expression for the anisotropy factor, $\mathcal{A} = k^2/\kappa^2$, into (9) gives the following:

$$\mathcal{K} = \frac{\mathcal{K}_0}{1 + \frac{\mathcal{A}}{\gamma^2\kappa^2}|\nabla Q|^2}. \tag{12}$$

Equation (12) demonstrates that the eddy diffusivity is suppressed not by the mean flow per se but by the presence of background PV gradients. The diffusivity is inversely proportional to the squared PV gradient (see also Nakamura and Zhu 2010b); the stronger the PV gradient, the stronger the suppression.

Equations (9) and (12) both describe suppression of eddy mixing, but offering different interpretations. Equation (9) expresses suppression in terms of the mean flow and the eddy phase speed, while (12) expresses the suppression in terms of the PV gradient directly. The 'velocity formulation' (9) has been used frequently before (Ferrari and Nikurashin 2010; Klocker et al. 2012), while the 'PV formulation' (12) was noted by Nakamura and Zhu (2010a) and Klocker et al. (2012). We use the PV form, recognizing that the mean velocity should drop out of the problem, due to the Galilean invariance noted earlier.

For simplicity, we focus on the f-plane case with a linear topographic PV gradient. Including the β-effect does not change the results qualitatively but merely requires rotating the coordinate system. The PV contours are thus parallel to the isobaths and $|\nabla Q| = \frac{f_0}{H}|\nabla h_b| \equiv \frac{f_0}{H}\alpha$. This yields an expression of the cross-slope diffusivity in terms of the topographic slope, α:

$$\mathcal{K} = \frac{\mathcal{K}_0}{1 + \frac{f_0^2\mathcal{A}}{\gamma^2\kappa^2H^2}\alpha^2}. \tag{13}$$

Note $\mathcal{K}$ is independent of the slope direction.

To evaluate the expression for $\mathcal{K}$, we require the wavenumber κ. We assume κ is given by $1/L$, where L is the dominant length scale of the eddies. We consider two options: the internal or first baroclinic Rossby radius, L_{Rossby}, and the topographic Rhines scale, L_{Rhines}. The first baroclinic

Rossby radius is given by:

$$L_{\text{Rossby}} \propto \frac{NH}{|f_0|}, \tag{14}$$

where N is the depth-averaged buoyancy frequency (e.g. Chelton et al. 1998). This is the approximate scale of the fastest growing mode in the Eady model for baroclinic instability (Eady 1949). Even though internal PV gradients (planetary β or layer thickness gradients) can introduce other scales (Charney 1947; Green 1960), L_{Rossby} remains a much used estimate of the eddy length scale (e.g. Hallberg 2013; LaCasce and Groeskamp 2020; Groeskamp et al. 2020). Of course the Rossby radius is relevant for a stratified flow whereas our derivation is based on the barotropic QGPV equation. The rationale is that the process setting the dominant wavelength is conversion of energy from the baroclinic to the barotropic mode, with the active dynamics then being barotropic (Larichev and Held 1995; Yankovsky et al. 2022).

Second, the topographic Rhines scale is given by:

$$L_{\text{Rhines}} \propto \sqrt{\frac{\mathcal{U}}{|\nabla Q|}} = \sqrt{\frac{\mathcal{U}}{f_0|\alpha|/H}}. \tag{15}$$

The topographic Rhines scale represents the maximum length scale in an inverse cascade and the transition between turbulence and topographic waves (e.g. Brink 2017). The 'standard' Rhines scale, which considers planetary Rossby waves instead of topographic waves and is equal to $\sqrt{\mathcal{U}/\beta}$ (Vallis and Maltrud 1993), is found to be a good estimate of the eddy mixing length scale (Thompson 2010; Stewart and Thompson 2016; Jansen et al. 2015, 2019; Kong and Jansen 2017). In studies focusing on continental shelves, Pringle (2001) and Brink (2017) used the topographic Rhines scale to represent the eddy wavelength. Jansen et al. (2015) and Grooms et al. (2015) suggested using the 'effective' Rhines scale, taking both planetary and topographic PV gradients into account by setting $|\nabla Q| = \left|\frac{f_0}{H}\nabla h_b + \beta_0 \hat{y}\right|$ in equation (15).

Taking $\kappa = 1/L_{\text{Rossby}}$ or $\kappa = 1/L_{\text{Rhines}}$ as estimates for the eddy wavenumber, (13) yields the following expressions for the eddy diffusivity:

$$\mathcal{K}_{\text{Rossby}} = \frac{\mathcal{K}_0}{1 + \frac{1}{\gamma^2}\frac{N^2H^2}{f_0^2}\mathcal{A}|\nabla Q|^2} = \frac{\mathcal{K}_0}{1 + \frac{1}{\gamma^2}\mathcal{A}N^2\alpha^2}, \tag{16}$$

$$\mathcal{K}_{\text{Rhines}} = \frac{\mathcal{K}_0}{1 + \frac{1}{\gamma^2}\mathcal{A}\mathcal{U}|\nabla Q|} = \frac{\mathcal{K}_0}{1 + \frac{1}{\gamma^2}\mathcal{A}\mathcal{U}\frac{|f_0|}{H}|\alpha|}. \tag{17}$$

With (16) and (17), we have two different analytical expressions for the cross-stream eddy diffusivity over a topographic slope, both of which indicate that topographic slopes suppress cross-isobath mixing. We proceed to test both expressions in a numerical model.

3. Validating theory in an idealized channel model

a. Numerical model description

We use the Bergen Layered Ocean Model (BLOM), the ocean component of the Norwegian Earth System Model (NorESM; Seland et al. 2020), in an idealized channel configuration. The simulations are described in Nummelin and Isachsen (2024) and we only give a brief summary here.

The model uses 51 isopycnal levels (potential density referenced to 2000 dbar) with a 2-level bulk mixed layer at the surface. The channel configuration is 416 km long in the zonal (x) direction and 1024 km wide in the meridional (y) direction with a 2 km resolution, and is re-entrant in the zonal direction. There are continental slopes of 2000 m extension from the shelf break at 250m to the bottom of the domain at 2250 m depth on both sides of the channel, centered at 150 km from the domain edge. To trigger instabilities we add white noise to the bottom topography with a standard deviation of 10 m. The channel is set up on the Northern Hemisphere f-plane. The model is initialized from rest with constant salinity and a horizontally homogeneous temperature profile. The density is determined by temperature alone, which has a maximum at the surface and decays exponentially towards the bottom. There is no buoyancy forcing (nor restoring) and we only force the flow with a constant westward wind stress. The surface mixed layer is kept shallow by parameterization of submesoscale mixed layer eddies (Fox-Kemper et al. 2008) that counter the vertical mixing induced by the constant wind forcing.

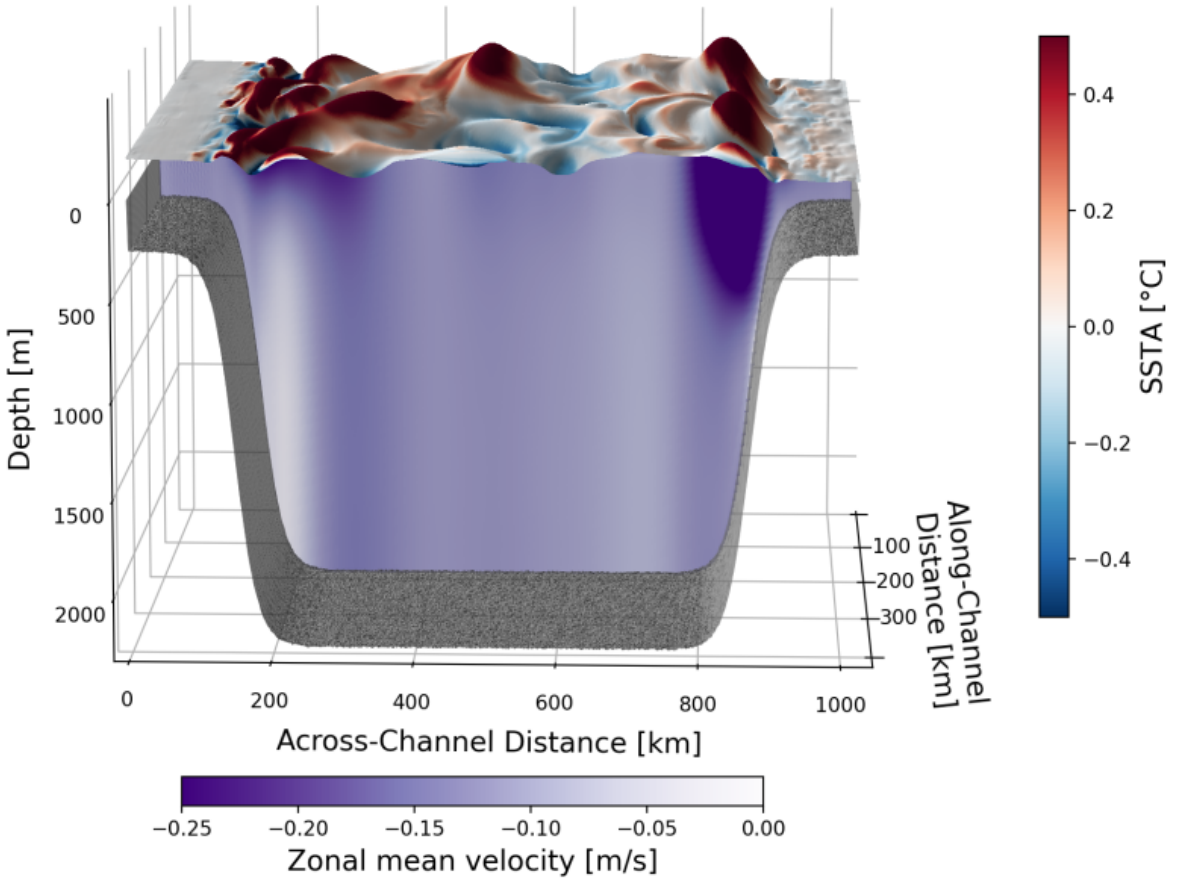

FIG. 1. Illustration of the channel model configuration. The surface elevations represent an exaggerated snapshot of daily SSH anomalies, with the colors showing a snapshot of daily SST anomalies. The purple hues show the zonal mean velocity.

The wind forcing drives a northward surface Ekman transport. Ekman divergence in the south and convergence in the north drive a westward mean flow, $U(y)$. The mean flow is retrograde with respect to topographic waves in the south whereas it is prograde in the north. Upwelling in the south establishes isopycnals that are sloping with the topography whereas downwelling in the north sets up isopycnals that slope against the topography. The tilted isopycnals in both regions are baroclinically unstable, creating an eddy field. Figure 1 shows a snapshot of the fields from one of the simulations.

We run 9 experiments, varying the initial stratification and the width of the continental slope, i.e the slope angle. The slope aspect ratio α = (slope height)/(slope width) varies between 0.016

and 0.027. These values are fairly representative for continental slopes (LaCasce 2017). All simulations are spun up for 10 years, to a semi-equilibrium where the kinetic energy has stabilized but still has some variability. The model fields are then diagnosed over an additional 5-year period (between years 11–15). The parameter settings and experiments are laid out in Tables 1 and 2, respectively.

TABLE 1. BLOM model constants for the channel simulations.

Name	Symbol	Value
Wind stress	τ_x	0.05 N m^{-2}
Horiz. grid size	$\Delta x, \Delta y$	2 km
Baroclinic timestep	Δt	120 s
Domain x-size	L_x	416 km
Domain y-size	L_y	1024 km
Gravitational acceleration	g	9.806 m s^{-2}
Coriolis parameter	f_0	1×10^{-4} s^{-1}
Slope mid-point distance from domain edge	Y_S	150 km
Shelf depth	H_{Shelf}	250 m
Slope height	H_{Slope}	2000 m

TABLE 2. Channel model experiments. L_{Rossby} is the mean deformation radius (equation 14) averaged over the last 5 years of the 15-year long experiments in the central basin (where the bottom depth is larger than 2250 m).

Name	L_{Rossby}	Slope Width	Slope Magnitude
Exp 1	34.1 ±1.3 km	75 km	0.027
Exp 2	34.1 ±1.1 km	100 km	0.020
Exp 3	34.4 ±1.0 km	125 km	0.016
Exp 4	30.6 ±1.3 km	75 km	0.027
Exp 5	30.6 ±1.2 km	100 km	0.020
Exp 6	30.4 ±1.0 km	125 km	0.016
Exp 7	24.9 ±1.2 km	75 km	0.027
Exp 8	25.9 ±1.0 km	100 km	0.020
Exp 9	24.9 ±1.0 km	125 km	0.016

b. Computing diffusivities from the model data

The goal is to compare cross-slope eddy diffusivities diagnosed from the model with the parameterizations from equations (16) and (17). We diagnose diffusivities using the flux-gradient relation $\mathcal{F}_C = -\mathcal{K}\nabla C$. As (16) and (17) were derived for a barotropic model, we first average the model

variables over depth. Then, we make a Reynolds decomposition of the tracer and velocity fields in the zonal (re-entrant) direction. We denote zonal mean fields with angle brackets (e.g. $\langle v \rangle$) and the eddy field (deviations from the zonal mean) with stars (e.g. $v^\star$). Diagnosing eddy diffusivities over bottom topography is typically done using spatial filtering because standing waves due to topography don't get detected when using Reynolds averaging (e.g. Khani et al. 2019; Buzzicotti et al. 2023; Xie et al. 2023). However, in our simulations we only have smooth topographic slopes without corrugations, and hence no standing waves. Therefore we assume that using Reynolds averaging in the zonal direction is justified here.

The cross-stream (y-direction) diffusivity of a tracer C is diagnosed from the depth-averaged tracer and cross-stream velocity fields using the flux-gradient relation:

$$\mathcal{K}^C_{\text{diag}} = -\frac{\langle v^\star C^\star \rangle}{\partial \langle C \rangle / \partial y}. \tag{18}$$

In the computation of (18), we select only those data points where the absolute value of the gradient $\partial \langle C \rangle / \partial y$ is larger than a threshold value, to avoid problems with unphysical diffusivity values. The choice of the threshold value mainly affects the diffusivity over the flat bottom, where gradients can become very small, while the impact over the slopes is limited. From the diffusivity values computed using (18), we select only the positive values. For the final analysis, $\mathcal{K}^C_{\text{diag}}$ is averaged over time, so that it is only a function of the cross-channel coordinate y. Formally, the parameterizations apply only to passive tracers, deriving as they do from the Taylor diffusivity (equation 8). However, we lack passive tracers in the present model simulations. Therefore we determined $\mathcal{K}_{\text{diag}}$ using two different tracers: temperature and (shallow water) PV, i.e. $(f+\zeta)/H$ with ζ the relative vorticity. The resulting diagnosed diffusivities are denoted as $\mathcal{K}^T_{\text{diag}}$ and $\mathcal{K}^{PV}_{\text{diag}}$, respectively. Neither temperature nor PV are necessarily passive, although they can be in certain situations (e.g. Larichev and Held 1995). The results turn out to be relatively insensitive to the chosen tracer.

To apply equations (16) and (17) to calculate parameterized eddy diffusivities from the numerical model data, we need to determine the eddy kinetic energy $\mathcal{U}^2$, the anisotropy factor $\mathcal{A}$, and the eddy decorrelation timescale γ. Both $\mathcal{U}^2$ and $\mathcal{A}$ can be expressed in terms of the eddy velocity field. Firstly, $\mathcal{U}^2$ is given by equation (7). Secondly, following Wei and Wang (2021) and using the monochromatic wave expression (3) for the eddy streamfunction, we can write the anisotropy

factor $\mathcal{A}$ as

$$\mathcal{A} = \frac{k^2}{k^2 + l^2} = \frac{\langle \psi_x'^2 \rangle}{\langle \psi_x'^2 \rangle + \langle \psi_y'^2 \rangle} = \frac{\left\langle v^{\star 2} \right\rangle}{\left\langle u^{\star 2} \right\rangle + \left\langle v^{\star 2} \right\rangle}. \tag{19}$$

It should be noted that most studies of mixing suppression assume that mesoscale eddies are horizontally isotropic, and hence that the anisotropy factor $\mathcal{A} = k^2/\kappa^2$ is equal to 1/2 everywhere (e.g. Ferrari and Nikurashin 2010; Naveira Garabato et al. 2011; Klocker et al. 2012; Chen et al. 2014, 2015; Griesel et al. 2015; Kong and Jansen 2017; Groeskamp et al. 2020). Wei and Wang (2021) concluded that eddies over topographic slopes are strongly anisotropic and as such that the anisotropy factor is important. We retain the term in our expression for $\mathcal{K}$ for completeness and analyze its importance later.

With equations (7) and (19), the unsuppressed diffusivity $\mathcal{K}_0$ can be written as $\mathcal{K}_0 = \mathcal{A}\mathcal{U}^2/\gamma = \left\langle v^{\star 2} \right\rangle / \gamma$, and equations (16) and (17) become

$$\mathcal{K}_{\text{Rossby}} = \left(1 + \frac{1}{\gamma^2} \frac{\left\langle v^{\star 2} \right\rangle}{\left\langle u^{\star 2} \right\rangle + \left\langle v^{\star 2} \right\rangle} N^2 \alpha^2 \right)^{-1} \frac{\left\langle v^{\star 2} \right\rangle}{\gamma}, \tag{20}$$

$$\mathcal{K}_{\text{Rhines}} = \left(1 + \frac{1}{\gamma^2} \frac{\left\langle v^{\star 2} \right\rangle}{\sqrt{\left\langle u^{\star 2} \right\rangle + \left\langle v^{\star 2} \right\rangle}} \frac{|f_0|}{H} |\alpha| \right)^{-1} \frac{\left\langle v^{\star 2} \right\rangle}{\gamma}. \tag{21}$$

Expressions (20) and (21) are computed from the depth and zonally averaged velocity fields, and averaged over time for the final analysis. For N in equation (20), we use the depth-averaged buoyancy frequency. The last parameter remaining is γ, the inverse eddy velocity decorrelation timescale. This represents damping due to nonlinear eddy-eddy interactions, and is usually left as a tunable parameter. Klocker and Abernathey (2014) found a good fit for diffusivity at the surface for $\gamma^{-1} = 4$ days, and Groeskamp et al. (2020) found $\gamma^{-1} = 1.68$ days for full-depth estimates. We explore the sensitivity of the parameterizations to γ subsequently.

c. Comparing parameterized and diagnosed diffusivities

Figure 2 shows the diagnosed and parameterized cross-slope diffusivities across the channel for all 9 experiments (Table 2). The diagnosed diffusivities $\mathcal{K}^T_{\text{diag}}$ and $\mathcal{K}^{PV}_{\text{diag}}$ are shown by the continuous and dashed black lines, respectively. Over the topographic slopes (gray shaded areas)

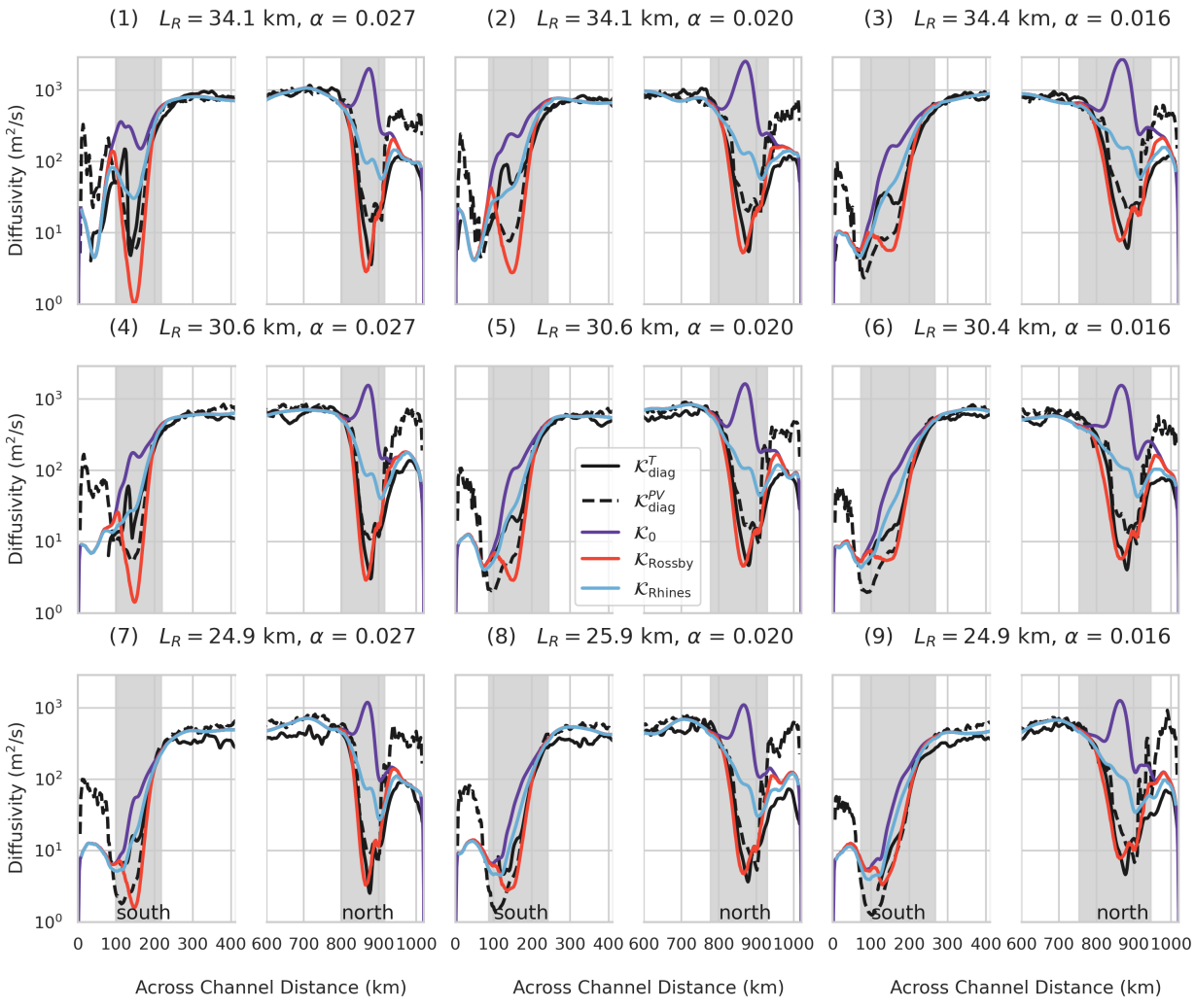

FIG. 2. Zonal and time mean depth-averaged cross-slope diffusivities across the channel for all 9 experiments from Table 2. Diffusivities are all plotted on a logarithmic scale. The continuous black line shows the diagnosed temperature diffusivity; the dashed black line shows the diagnosed PV diffusivity; the purple line shows the parameterized unsuppressed diffusivity from equation (10); the red and blue lines show the parameterized diffusivities from equations (20) and (21), respectively. The parameterized diffusivities are all shown for $\gamma^{-1} = 4$ days. The mid-basin part between 400 and 600 km is not shown; here the diffusivity is approximately constant. The gray shaded areas indicate the topographic slopes.

they are suppressed compared to the flat mid-basin by 2–3 orders of magnitude. Over the northern (prograde) slope, $\mathcal{K}^T_{\text{diag}}$ and $\mathcal{K}^{PV}_{\text{diag}}$ are very similar across all experiments; over the southern (retrograde) slope they exhibit differences for some experiments, with $\mathcal{K}^T_{\text{diag}}$ showing local maxima.

The reason for this is that the wind forcing induces northward Ekman transport, so that the cross-channel temperature gradient $\partial T/\partial y$ becomes small in the south, hence $\mathcal{K}^T_{\text{diag}}$ becomes large (equation 18).

Next, the purple, red and blue lines show the parameterized diffusivities $\mathcal{K}_0$, $\mathcal{K}_{\text{Rossby}}$ and $\mathcal{K}_{\text{Rhines}}$, respectively. Each of these employ $\gamma^{-1} = 4$ days; this produces good agreement between the parameterized and diagnosed diffusivities in the mid-basin, but we will discuss the impact of γ below. Looking first at the parameterized unsuppressed diffusivity $\mathcal{K}_0$ (equation 10), we see that it is weaker in the south than in the mid-basin, but overestimates $\mathcal{K}^T_{\text{diag}}$ there. Over the northern slope, $\mathcal{K}_0$ has a maximum, and becomes even stronger than in the mid-basin. The reason is that eddy kinetic energy is enhanced over the northern slope (not shown). Focusing on our paremeterizations that account for topographic PV gradients, $\mathcal{K}_{\text{Rossby}}$ and $\mathcal{K}_{\text{Rhines}}$, we see that both are suppressed over the slopes and are much better approximations of the diagnosed diffusivity. Over the southern (retrograde) slope, $\mathcal{K}_{\text{Rhines}}$ matches well with $\mathcal{K}^T_{\text{diag}}$, whereas $\mathcal{K}_{\text{Rossby}}$ is closer to $\mathcal{K}^{PV}_{\text{diag}}$. Over the northern (prograde) slope, $\mathcal{K}_{\text{Rhines}}$ overestimates both diagnosed diffusivities, while $\mathcal{K}_{\text{Rossby}}$ closely follows the profile of $\mathcal{K}^T_{\text{diag}}$. The reduction by 2–3 orders of magnitude of the diagnosed diffusivity over the slopes is captured by both $\mathcal{K}_{\text{Rossby}}$ and $\mathcal{K}_{\text{Rhines}}$ over the southern slope and by $\mathcal{K}_{\text{Rossby}}$ over the northern slope. So, despite the QG assumptions not being valid everywhere in the present model setting (e.g. $|h_b| \ll H$), our parameterizations still produce results that are in fairly good agreement with the diagnosed diffusivity behavior.

Figure 3 explores the relevance of the anisotropy factor $\mathcal{A}$ in the parameterized diffusivities. The value of $\mathcal{A}$ changes from 0.6 (close to isotropic) over the flat mid-basin to 0.1 (0.2) over the northern (southern) slopes. Although this is a notable change, it is still small compared to the observed 2–3 orders of magnitude change in diffusivities over the slopes. In other words, it is the presence of α rather than $\mathcal{A}$ in the suppression factor that is responsible for most of the suppression over the slopes. Figure 3 shows that using constant or non-constant $\mathcal{A}$ yields very similar diffusivity profiles for experiment 8 from Table 2; this result holds across all experiments.

Figure 4 shows the profiles of the parameterized diffusivities $\mathcal{K}_{\text{Rossby}}$ and $\mathcal{K}_{\text{Rhines}}$ for a wide range of values of the eddy decorrelation timescale γ^{-1}. The dependence on γ is strongest for small γ^{-1}, whereas it becomes weak for large γ^{-1}. We see that the value of γ^{-1} that gives the best agreement differs between the two parameterizations and also between the northern slope, southern slope

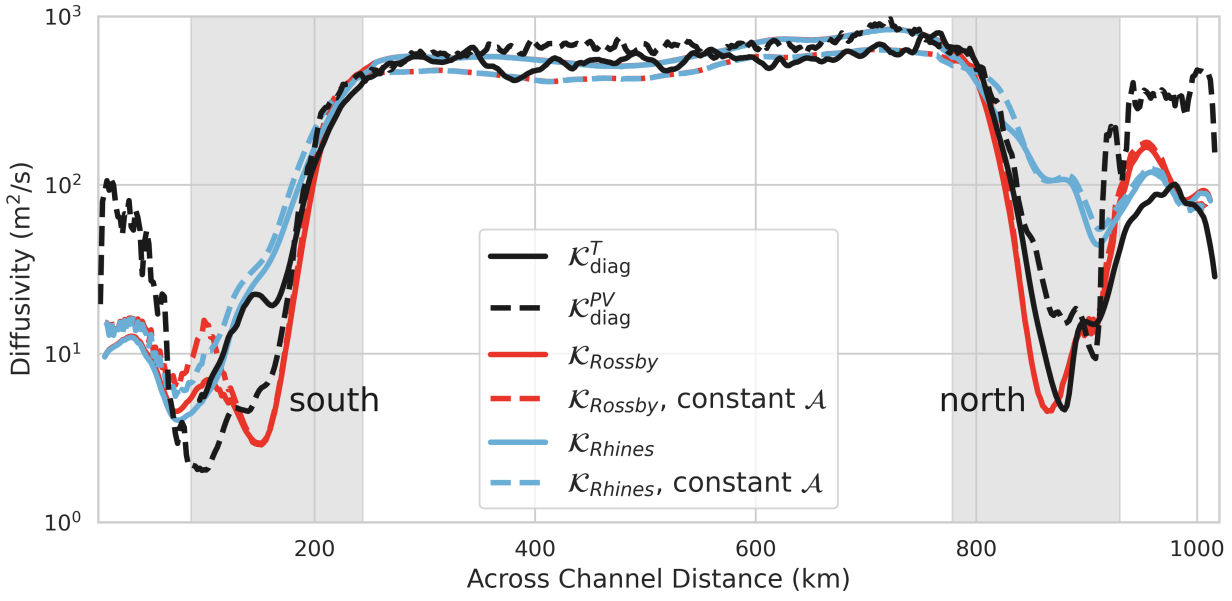

FIG. 3. Diagnosed and parameterized diffusivities (as in Figure 2) for experiment 5 from Table 2. Diffusivities are all plotted on a logarithmic scale. The dashed lines show the parameterized diffusivities with a constant anisotropy factor $\mathcal{A}$, taken to be the mean cross-basin value.

and flat-bottomed mid-basin. For small values of γ^{-1}, the parameterizations underestimate the diagnosed diffusivities in the mid-basin but overestimate diffusivities over the northern slope, with $\mathcal{K}_{\text{Rhines}}$ showing local maxima over the northern slope, approaching $\mathcal{K}_0$ (Figure 2). For larger values of γ^{-1}, the parameterized diffusivity profiles converge, but overestimate the diagnosed diffusivities in the mid-basin. $\mathcal{K}_{\text{Rossby}}$ matches best with the diagnosed diffusivities for values of γ^{-1} around 2–4 days. On the other hand, $\mathcal{K}_{\text{Rhines}}$ is relatively insensitive to the value of γ^{-1} over the southern slope, but performs best for high values of γ^{-1} over the northern slope. Note the exact value of γ^{-1} will vary depending on approximations, e.g. neglecting factors of π in the various expressions for length and time scales.

4. Discussion

a. Relevance of eddy length and time scales

In the derivation of (12), it is assumed that mesoscale eddies can be described as monochromatic waves with all energy at a single wavenumber. In reality, the oceanic eddy field contains motions

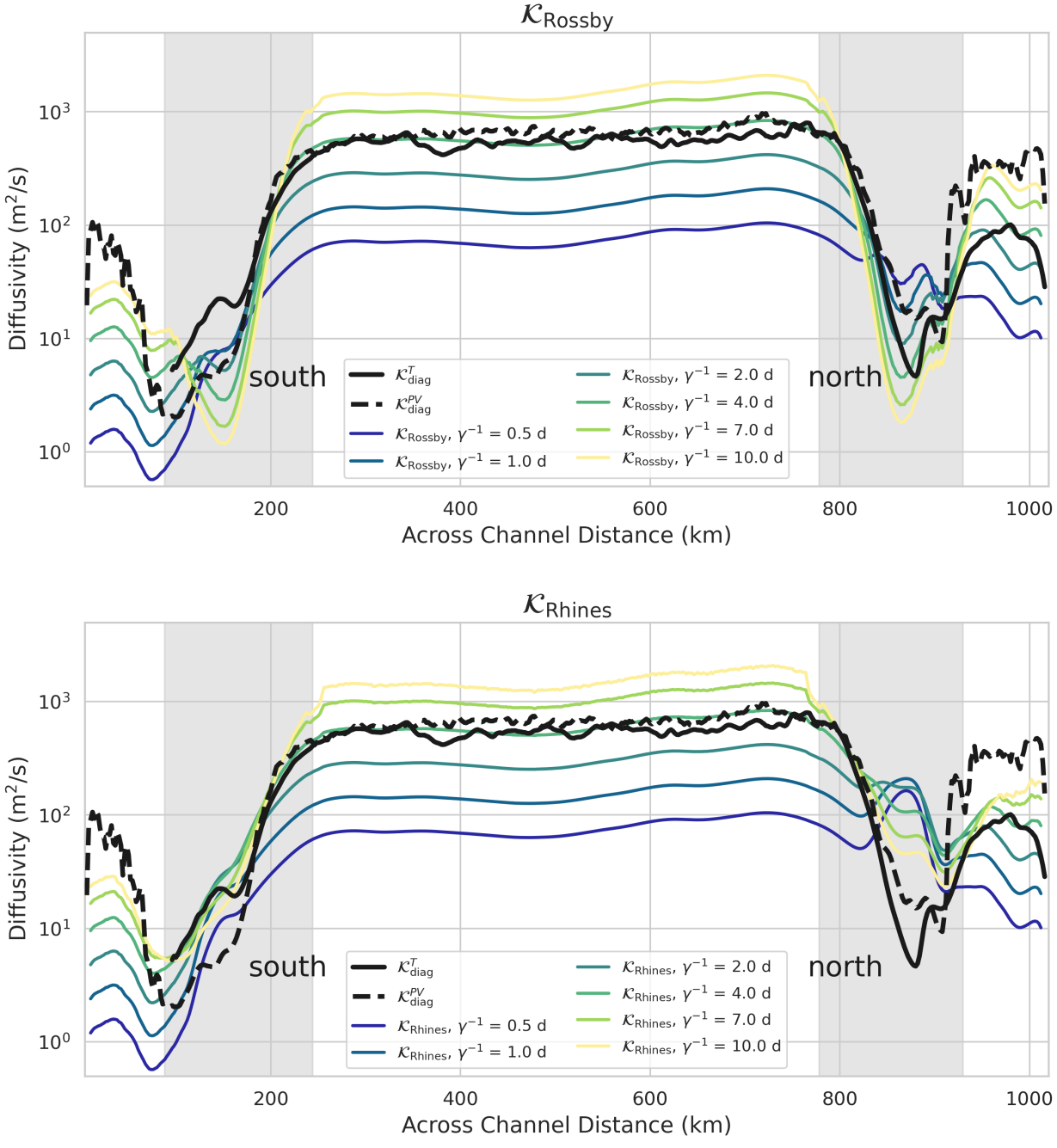

FIG. 4. Parameterized diffusivities $\mathcal{K}_{\text{Rossby}}$ (equation 20) and $\mathcal{K}_{\text{Rhines}}$ (equation 21) for different values of γ and diagnosed diffusivities $\mathcal{K}^T_{\text{diag}}$ and $\mathcal{K}^{PV}_{\text{diag}}$, shown for experiment 5 from Table 2. The values of γ^{-1} are indicated in days. Diffusivities are all plotted on a logarithmic scale.

over a broad range of wavenumbers (Wunsch 2010; Wortham and Wunsch 2014). A number of studies have derived eddy diffusivity parameterizations for multichromatic waves. Chen et al. (2015)

developed a multi-wavenumber theory for eddy diffusivities, but only considered wavenumbers in the along-stream direction. Kong and Jansen (2017) considered the full two-dimensional EKE spectrum to compute eddy diffusivities, but assumed isotropy. Instead, like most other studies, we retained the assumption of monochromatic waves. We considered two different length scales to set the dominant wavelength: the Rossby radius and the topographic Rhines scale. As seen in Figure 2, we find good agreement between theory and model results in both cases. This suggests that the assumption of monochromatic waves works well with a realistic value for the most energetic eddy length scale for this model.

Other studies have not yet provided a clear conclusion on which length scale best represents eddy mixing length over topographic slopes. Wang and Stewart (2020) and Wei et al. (2022) found that the topographic Rhines scale works well to parameterize eddy diffusivity over retrograde slopes, but that it is not suitable for prograde slopes in a stratified ocean. On the other hand, Wei and Wang (2021) parameterized diffusivities over retrograde slopes using the Rossby radius, and found that the topographic Rhines scale led to an overestimation of the diagnosed diffusivity. These findings suggest differences in eddy length scales between prograde and retrograde slopes. In our simulations, a relevant difference between the two slopes is that EKE is enhanced over the northern (prograde) slope due to Ekman downwelling, but weakened in the south due to Ekman upwelling. Over the southern (retrograde) slope, the suppression of the eddy diffusivity is already captured quite well by $\mathcal{K}_0$, which takes into account EKE but not topographic PV gradients. Hence, in this upwelling region, the weakened EKE already contains a large part of the suppression. On the other hand, over the northern (prograde) slope the topographic PV gradient is needed to represent the suppression effect. Here, an important difference between the two length scales is that $\mathcal{K}_{\text{Rhines}}$ is inversely proportional to the PV gradient, whereas $\mathcal{K}_{\text{Rossby}}$ is inversely proportional to the PV gradient squared. The importance of the squared PV gradient (the bottom slope) was noted in Nummelin and Isachsen (2024) and previous studies, suggesting that the Rossby radius might be the more appropriate length scale to use. This will be further discussed in Section 4b. Finally, in the simulations used in this study, the eddies have a size in the order of the Rossby radius (not shown), whereas the topographic Rhines scale is an order of magnitude too small. This further supports the conclusion that the Rossby radius is the appropriate eddy length scale for the simulations presented here.

Regarding the eddy velocity decorrelation timescale, there are, to the best of our knowledge, no observational studies on the values of γ in the ocean. As noted, γ is typically left as an adjustable parameter when computing eddy diffusivities (e.g. Klocker and Abernathey 2014; Groeskamp et al. 2020). The value of γ could possibly be inferred from an inverse method, like that employed in Mak et al. (2022a) for the mesoscale eddy energy dissipation timescale. Another option could be to determine γ from the autocorrelation of observational velocity timeseries. Our results suggest γ varies depending on the relevant dynamics in a region, and this should be examined further.

b. Relation with empirical expressions for eddy diffusivity

Among others, Brink (2012), Brink and Cherian (2013), Brink (2016) and Wei et al. (2022) have constructed an empirical scaling for eddy diffusivity in terms of the slope Burger number, $\mathcal{S} = \alpha N / f_0$. They all give parameterizations for $\mathcal{K}$ of the form

$$\mathcal{K} = \frac{\mu}{1 + \eta S^{\varepsilon}}, \quad S = \frac{\alpha N}{f_0}. \tag{22}$$

The values of the parameters μ and η and the exponent ε vary between these studies. The general form of (22) is the same as our expression for $\mathcal{K}_{\text{Rossby}}$, equation (16), if the factor f_0 in S is replaced by the eddy decorrelation timescale γ. The exponent ε in our case is equal to 2, which is the same as in Brink and Cherian (2013) and Brink (2016) (by contrast, Brink (2012) found $\varepsilon = 1$, whereas Wei et al. (2022) reported $\varepsilon = 1.4$). This means that our parameterization using the Rossby radius, which is dynamically based, is consistent with the previously found empirically based expressions for eddy diffusivities over topographic slopes.

c. Challenges for implementation in coarse-resolution climate models

One of the main reasons to study eddy diffusivities over topographic slopes is to create better parameterizations for coarse-resolution climate models. Using (13) with the appropriate length scale to compute eddy diffusivities requires knowledge on the eddy kinetic energy $\mathcal{U}^2$, the eddy anisotropy factor $\mathcal{A}$, and the eddy velocity decorrelation timescale γ. Here we expressed $\mathcal{U}^2$ and $\mathcal{A}$ in terms of the eddy velocity field and used the resulting expressions (20) and (21) to compute eddy diffusivities from the numerical model's depth-averaged flow field data, leaving γ as an adjustable parameter (Section 3b). However, expressions (20) and (21) are not suitable for implementation

in climate models. The reason is the lack of closures for the eddy-related parameters $\mathcal{U}^2$, $\mathcal{A}$ and γ, which depend on properties below the typical grid scale of coarse-resolution climate models. Closures and parameterizations of eddy kinetic energy are an active research topic (e.g. Eden and Greatbatch 2008; Jansen et al. 2015, 2019; Mak et al. 2017, 2018; Juricke et al. 2020a,b). Wei and Wang (2021) present a parameterization for the anisotropy factor, though the derivation is empirical. Note, though, that in our simulations, it is the topographic PV gradient rather than the anisotropy factor that causes most of the suppression of the depth-averaged diffusivity (see also Nummelin and Isachsen 2024). It is therefore a reasonable approximation to simplify the expressions by assuming a constant anisotropy factor. Regarding the eddy decorrelation timescale, more research is needed for determining prognostic equations for γ, as discussed in Section 4a. Furthermore, a shortcoming of the parameterizations presented here is that they do not take into account baroclinic effects and hence cannot be used to get vertical profiles of the eddy diffusivity. Adding stratification greatly increases the complexity of the problem, which can already be seen in a two-layer model (e.g. Straub 1994; Boland et al. 2012). Moreover, a varying anisotropy factor might be important for the vertical structure of eddy diffusivities (Stewart et al. 2015; Wei and Wang 2021), so assuming constant anisotropy is then no longer a good approximation. Nevertheless, with appropriate estimates for $\mathcal{U}^2$, $\mathcal{A}$, and γ, we still consider expression (13) of value for testing in climate models to represent depth-averaged eddy diffusivities.

d. Applicability of results for observations

The skill of parameterizations (20) and (21) in reproducing eddy diffusivities in a numerical model also motivates application to observational data. Direct observations of mesoscale eddy mixing can be made in tracer release experiments (Ledwell et al. 1993, 1998; Tulloch et al. 2014; Zika et al. 2020; Bisits et al. 2023), but these experiments are expensive and labor intensive, and only provide information about a specific region. By contrast, our parameterizations could be used to infer eddy diffusivity values from more easily attainable observations. Groeskamp et al. (2020) applied the velocity formulation from Ferrari and Nikurashin (2010) to an observation-based gridded ocean climatology to create full-depth global estimates of eddy diffusivities. However, the expression of Ferrari and Nikurashin (2010) does not include effects of topographic PV gradients. Moreover, it requires fitting of the eddy decorrelation timescale γ, and approximating the total

eddy phase speed c_w. Table 4 of Wei and Wang (2021) summarizes the methods that different studies used to determine c_w, which include empirical fits to numerical model results (e.g. Klocker et al. 2012; Pennel and Kamenkovich 2014), linear stability analysis (e.g. Eden 2011; Griesel et al. 2015), the use of SSH measurements (e.g. Ferrari and Nikurashin 2010; Naveira Garabato et al. 2011; Sallée et al. 2011; Abernathey and Marshall 2013; Bates et al. 2014; Klocker and Abernathey 2014; Balwada et al. 2016; Roach et al. 2016, 2018; Bolton et al. 2019; Busecke and Abernathey 2019; Groeskamp et al. 2020), or simply assuming $c_w \approx 0$ (e.g. Meredith et al. 2012; Bire and Wolfe 2018). By contrast, in the PV formulation the term $c_w - U$ is replaced by c, the intrinsic eddy phase speed, for which we have an analytical expression in terms of the background (planetary and topographic) PV gradient. Thus, in the barotropic case we can calculate c in a straightforward way from β and the topographic slope, and circumvent the problem of having to determine c_w. In the end, the only observational measurements that our equations (20) and (21) require are information on stratification, topographic slopes, and flow velocity timeseries (for $\mathcal{A}$, $\mathcal{U}^2$ and γ); one could obtain these from mooring data. Within the assumptions made here, this provides a new and improved method to estimate depth-averaged eddy diffusivities based on oceanographic measurements, and thus to study variability in eddy diffusivity across the ocean.

5. Summary and Conclusion

We derived an analytical expression, equation (13), to describe depth-averaged eddy diffusivities over topographic slopes (Figure 2). This expression is a specific case of the general equation (12) for the cross-stream eddy diffusivity in the presence of a background PV gradient. Equation (12) explicitly links eddy diffusivity to the PV gradient (Nakamura and Zhu 2010b), thus providing a PV formulation of mixing suppression, as opposed to the velocity formulation (9) presented in previous studies (e.g. Ferrari and Nikurashin 2010; Klocker et al. 2012). An advantage of the PV formulation is that it does not require information on c_w, the Doppler-shifted or apparent phase speed of the eddies, and U, the background mean flow. We circumvent the problem of having to determine c_w and U and instead keep an analytical expression for the intrinsic eddy phase speed, which is linked to the PV gradient. Furthermore, keeping the PV gradient ∇Q in the expression for $\mathcal{K}$, we can substitute exact expressions for ∇Q to see which physical mechanisms determine $\mathcal{K}$. Many studies on mixing suppression in the ACC assume the PV gradient is set by planetary

β (e.g. Ferrari and Nikurashin 2010; Naveira Garabato et al. 2011; Klocker et al. 2012; Griesel et al. 2015). Instead, the main focus of this study was the influence of bottom topography on eddy mixing. Across the world's oceans the topographic PV gradient is typically larger than the planetary PV gradient (with the exception of low latitudes). Equation (13) directly relates the eddy diffusivity to the topographic slope α. This equation is not based on empirical fits to model results, but on physically consistent derivations that include topography from the start. Finally, our parameterization can be calculated from velocity timeseries, presenting a new opportunity for computing eddy diffusivities from observational data.

A number of issues still remain to be addressed. Closures for the eddy anisotropy, EKE, and decorrelation timescale are missing; the physical mechanisms setting the eddy length scale in different dynamical regimes require further study; and the parameterizations for $\mathcal{K}$ presented in this study do not take into account baroclinic effects. Nevertheless, the parameterizations help in understanding the physical mechanism of mixing suppression by topography, and can accurately represent depth-averaged eddy diffusivities in an idealized simulation. This motivates future studies to extend the parameterizations to a baroclinic (depth-varying) framework, and to explore the applicability of the parameterizations for computing eddy diffusivities from observations and models.

Author contributions. **MFS:** Conceptualization, Methodology, Formal analysis, Writing - Original Draft. **JHL:** Conceptualization, Methodology. **SG:** Conceptualization, Methodology, Supervision, Project administration, Funding acquisition. **AN:** Software, Formal analysis, Resources. **PEI:** Resources. **MLJB:** Supervision, Project administration, Funding acquisition. **Everyone:** Writing - Review & Editing.

Acknowledgments. MFS was funded by the UU-NIOZ project "The intermittency of large-scale ocean mixing" (project number NZ4543.3). JHL was supported under project number 302743 (the Rough Ocean) of the Norwegian Research Council. AN and PEI were funded by the two Research Council of Norway projects KeyClim (295046) and TopArctic (314826). MLJB was funded by the program of the Netherlands Earth System Science Centre (NESSC), financially supported by the Ministry of Education, Culture and Science (OCW, grant number 024.002.001). The model simulations and storage were performed on resources provided by Sigma2 - the National Infrastructure for High Performance Computing and Data Storage in Norway under the accounts NN9252K, NS9252K, NN9869K, and NS9869K. We thank Julian Mak and one anonymous reviewer for their thorough and helpful reviews of the manuscript.

Data availability statement. The model configuration and namelists needed for reproducing the results are published in Zenodo (Nummelin 2023b) and available at `https://doi.org/10.5281/zenodo.8227381`. The key model outputs (Nummelin 2023a) needed for reproducing the analysis are published at the NIRD research data archive and available at `https://archive.sigma2.no/pages/public/datasetDetail.jsf?id=10.11582/2023.00129`. Scripts for data processing and plotting can be shared upon request.

APPENDIX A

Derivation of expression for cross-stream eddy diffusivity

To compute the cross-stream eddy diffusivity, we need an analytical expression for the eddy streamfunction ψ'. We express ψ' as a Rossby wave (equation 3). Combining equations (4) and (6), we get a differential equation for the wave amplitude $a(t)$:

$$\frac{da}{dt} + (\gamma + ikc_w)a \equiv \frac{da}{dt} + \lambda a = Ar(t). \tag{A1}$$

To solve (A1), we use an integrating factor $e^{\lambda t}$:

$$\left(\frac{\mathrm{d}a}{\mathrm{d}t} + \lambda a\right) e^{\lambda t} = \frac{\mathrm{d}}{\mathrm{d}t}\left(a(t)e^{\lambda t}\right) = Ar(t)e^{\lambda t}. \tag{A2}$$

For a full solution, we need an initial condition. For this, we assume that we started out in a state of rest, i.e. $\lim_{t\to-\infty} a(t) = 0$. This gives us the solution

$$a(t) = A\int_{-\infty}^{t} r(\tau)e^{\lambda(\tau-t)}\mathrm{d}\tau. \tag{A3}$$

Now we need to determine the forcing amplitude A. We do this using the eddy kinetic energy (EKE), given by

$$\mathrm{EKE} = \frac{1}{2}\left\langle u'^2 + v'^2\right\rangle = \frac{1}{2}\left\langle \left|\psi'_x\right|^2 + \left|\psi'_y\right|^2\right\rangle = \frac{1}{2}\left\langle \kappa^2|\psi'|^2\right\rangle = \frac{1}{2}\left\langle \kappa^2|a|^2\right\rangle \equiv \frac{1}{2}\mathcal{U}^2, \tag{A4}$$

where $\langle\cdot\rangle$ denotes a time average. Using expression (A3) for $a(t)$, we find

$$|a|^2 = aa^* = A^2\int_{-\infty}^{t}\int_{-\infty}^{t} r(\tau)r^*(\tau)e^{\lambda(\tau-t)+\lambda^*(\tau'-t)}\mathrm{d}\tau'\mathrm{d}\tau, \tag{A5}$$

where * denotes complex conjugate. Since $r(t)$ is a white noise random process, $\langle r(\tau)r^*(\tau')\rangle = \delta(\tau-\tau')$. Furthermore, $\lambda \equiv \gamma + ikc_w$, so $\lambda + \lambda^* = 2\gamma$. This yields

$$\left\langle |a|^2\right\rangle = A^2\int_{-\infty}^{t} e^{2\gamma(\tau-t)}\mathrm{d}\tau = \frac{A^2}{2\gamma}. \tag{A6}$$

Combining this with the expression for the EKE, (A4), gives an expression for the stochastic forcing amplitude A:

$$A = \frac{\sqrt{2\gamma}\mathcal{U}}{\kappa}. \tag{A7}$$

Combining equations (3), (A3) and (A7) gives us the following expression for the eddy stream-function:

$$\psi'(x,y,t) = \mathrm{Re}\left(\frac{\sqrt{2\gamma}}{\kappa}\mathcal{U}e^{ikx+ily}\int_{-\infty}^{t} r(\tau)e^{\lambda(\tau-t)}\mathrm{d}\tau\right). \tag{A8}$$

We can use (A8) to get an expression for v', which is needed to compute the Taylor diffusivity, given by equation (8). We approximate the Lagrangian velocity v_L with the Eulerian velocity of a particle advected by the mean flow (leaving out Re for simplicity in the notation):

$$v_L(t;x,y,0) = v'(x+Ut,y,t) = \left.\frac{\partial\psi'}{\partial x}\right|_{(x+Ut,y,t)} = a(t)ike^{ik(x+Ut)+ily}. \tag{A9}$$

The autocorrelation of the cross-stream Lagrangian velocity R_{vv} is now given by

$$R_{vv} = \frac{2\gamma\mathcal{U}^2k^2}{\kappa^2}e^{ikU(t-t')-\lambda t-\lambda^* t'}\int_{-\infty}^{t}\int_{-\infty}^{t'} r(\tau)r^*(\tau')e^{\lambda\tau+\lambda^*\tau'}\mathrm{d}\tau'\mathrm{d}\tau. \tag{A10}$$

When taking the average $\langle R_{vv}\rangle$, as is needed for (8), we can again use that $\langle r(\tau)r^*(\tau')\rangle = \delta(\tau-\tau')$. This gives us

$$\langle R_{vv}\rangle = \frac{2\gamma\mathcal{U}^2k^2}{\kappa^2}e^{ikU(t-t')-\lambda t-\lambda^* t'}\int_{-\infty}^{t}\int_{-\infty}^{t'} \delta(\tau-\tau')e^{\lambda\tau+\lambda^*\tau'}\mathrm{d}\tau'\mathrm{d}\tau. \tag{A11}$$

The solution to the integral is (using that $\lambda+\lambda^* = 2\gamma$):

$$\int_{-\infty}^{t}\int_{-\infty}^{t'} \delta(\tau-\tau')e^{\lambda\tau+\lambda^*\tau'}\mathrm{d}\tau'\mathrm{d}\tau = \frac{1}{2\gamma}\left[\theta(t'-t)\left(e^{2\gamma t}-e^{2\gamma t'}\right)+e^{2\gamma t'}\right], \tag{A12}$$

where θ is the Heaviside step function (equal to zero for negative arguments and to one for positive arguments). In (8) we integrate over t' from 0 to t, meaning that t' must be smaller than t. So

$\theta(t'-t)=0$, and (A12) reduces to

$$\int_{-\infty}^{t}\int_{-\infty}^{t'}\delta(\tau-\tau')e^{\lambda\tau+\lambda^*\tau'}\mathrm{d}\tau'\mathrm{d}\tau=\frac{1}{2\gamma}e^{2\gamma t'}. \tag{A13}$$

So (A11) becomes

$$\langle R_{vv}\rangle=\frac{\mathcal{U}^2k^2}{\kappa^2}e^{ik(c_w-U)(t'-t)}e^{\gamma(t'-t)}, \tag{A14}$$

where we used $\lambda=\gamma+ikc_w$ and $c_w=U+c$. Now we integrate over the real part of $\langle R_{vv}\rangle$ to compute the diffusivity as in (8):

$$\mathcal{K}=\lim_{t\to\infty}\frac{\mathcal{U}^2k^2}{\kappa^2}\int_0^t e^{\gamma(t'-t)}\cos\left[k(c_w-U)(t'-t)\right]\mathrm{d}t'. \tag{A15}$$

We can solve this integral using the substitution $\sigma=t'-t$ (and $c_w-U=c$):

$$\mathcal{K}=\lim_{t\to\infty}\frac{\mathcal{U}^2k^2}{\kappa^2\left(\gamma^2+c^2k^2\right)}\left[\gamma-e^{-\gamma t}\left(\gamma\cos(ckt)-ck\sin(ckt)\right)\right]. \tag{A16}$$

Finally we take the limit of $t\to\infty$ to find the diffusivity in an equilibrium situation:

$$\mathcal{K}=\frac{k^2}{\kappa^2}\frac{\gamma\mathcal{U}^2}{\gamma^2+c^2k^2}=\frac{k^2}{\kappa^2}\frac{\gamma\mathcal{U}^2}{\gamma^2+(c_w-U)^2k^2}=\frac{\mathcal{A}\mathcal{U}^2/\gamma}{1+\frac{k^2}{\gamma^2}(c_w-U)^2}. \tag{A17}$$

References

Abernathey, R. P., and J. Marshall, 2013: Global surface eddy diffusivities derived from satellite altimetry. *Journal of Geophysical Research: Oceans*, **118 (2)**, 901–916, https://doi.org/10.1002/jgrc.20066.

Balwada, D., K. G. Speer, J. H. LaCasce, W. B. Owens, J. Marshall, and R. Ferrari, 2016: Circulation and Stirring in the Southeast Pacific Ocean and the Scotia Sea Sectors of the Antarctic Circumpolar Current. *Journal of Physical Oceanography*, **46 (7)**, 2005–2027, https://doi.org/10.1175/JPO-D-15-0207.1.

Bates, M., R. Tulloch, J. Marshall, and R. Ferrari, 2014: Rationalizing the Spatial Distribution of Mesoscale Eddy Diffusivity in Terms of Mixing Length Theory. *Journal of Physical Oceanography*, **44 (6)**, 1523–1540, https://doi.org/10.1175/JPO-D-13-0130.1.

Bire, S., and C. L. P. Wolfe, 2018: The Role of Eddies in Buoyancy-Driven Eastern Boundary Currents. *Journal of Physical Oceanography*, **48 (12)**, 2829–2850, https://doi.org/10.1175/JPO-D-18-0040.1.

Bisits, J. I., G. J. Stanley, and J. D. Zika, 2023: Can We Accurately Quantify a Lateral Diffusivity from a Single Tracer Release? *Journal of Physical Oceanography*, **53 (2)**, 647–659, https://doi.org/10.1175/JPO-D-22-0145.1.

Boland, E. J. D., A. F. Thompson, E. Shuckburgh, and P. H. Haynes, 2012: The Formation of Nonzonal Jets over Sloped Topography. *Journal of Physical Oceanography*, **42 (10)**, 1635–1651, https://doi.org/10.1175/JPO-D-11-0152.1.

Bolton, T., R. Abernathey, and L. Zanna, 2019: Regional and Temporal Variability of Lateral Mixing in the North Atlantic. *Journal of Physical Oceanography*, **49 (10)**, 2601–2614, https://doi.org/10.1175/JPO-D-19-0042.1.

Brink, K. H., 2012: Baroclinic instability of an idealized tidal mixing front. *Journal of Marine Research*, **70 (4)**, 661–688, https://doi.org/10.1357/002224012805262716.

Brink, K. H., 2016: Continental Shelf Baroclinic Instability. Part I: Relaxation from Upwelling or Downwelling. *Journal of Physical Oceanography*, **46 (2)**, 551–568, https://doi.org/10.1175/JPO-D-15-0047.1.

Brink, K. H., 2017: Surface Cooling, Winds, and Eddies over the Continental Shelf. *Journal of Physical Oceanography*, **47 (4)**, 879–894, https://doi.org/10.1175/JPO-D-16-0196.1.

Brink, K. H., and D. A. Cherian, 2013: Instability of an idealized tidal mixing front: Symmetric instabilities and frictional effects. *Journal of Marine Research*, **71 (6)**, 425–450, https://doi.org/10.1357/002224013812587582.

Busecke, J. J. M., and R. P. Abernathey, 2019: Ocean mesoscale mixing linked to climate variability. *Science Advances*, **5 (1)**, eaav5014, https://doi.org/10.1126/sciadv.aav5014.

Buzzicotti, M., B. A. Storer, H. Khatri, S. M. Griffies, and H. Aluie, 2023: Spatio-Temporal Coarse-Graining Decomposition of the Global Ocean Geostrophic Kinetic Energy. *Journal of Advances in Modeling Earth Systems*, **15 (6)**, e2023MS003 693, https://doi.org/10.1029/2023MS003693.

Canuto, V. M., Y. Cheng, A. M. Howard, and M. S. Dubovikov, 2019: Three-Dimensional, Space-Dependent Mesoscale Diffusivity: Derivation and Implications. *Journal of Physical Oceanography*, **49 (4)**, 1055–1074, https://doi.org/10.1175/JPO-D-18-0123.1.

Chapman, C., and J.-B. Sallée, 2017: Isopycnal Mixing Suppression by the Antarctic Circumpolar Current and the Southern Ocean Meridional Overturning Circulation. *Journal of Physical Oceanography*, **47 (8)**, 2023–2045, https://doi.org/10.1175/JPO-D-16-0263.1.

Charney, J. G., 1947: The Dynamics of Long Waves in a Baroclinic Westerly Current. *Journal of Meteorology*, **4 (5)**, 136–162, https://doi.org/10.1175/1520-0469(1947)004⟨0136:TDOLWI⟩2.0.CO;2.

Chelton, D. B., R. A. deSzoeke, M. G. Schlax, K. El Naggar, and N. Siwertz, 1998: Geographical Variability of the First Baroclinic Rossby Radius of Deformation. *Journal of Physical Oceanography*, **28 (3)**, 433–460, https://doi.org/10.1175/1520-0485(1998)028⟨0433:GVOTFB⟩2.0.CO;2.

Chelton, D. B., M. G. Schlax, and R. M. Samelson, 2011: Global observations of nonlinear mesoscale eddies. *Progress in Oceanography*, **91 (2)**, 167–216, https://doi.org/10.1016/j.pocean.2011.01.002.

Chen, R., S. T. Gille, J. L. McClean, G. R. Flierl, and A. Griesel, 2015: A multiwavenumber theory for eddy diffusivities and its application to the Southeast Pacific (DIMES) Region. *Journal of Physical Oceanography*, **45 (7)**, 1877–1896, https://doi.org/10.1175/JPO-D-14-0229.1.

Chen, R., J. L. McClean, S. T. Gille, and A. Griesel, 2014: Isopycnal Eddy Diffusivities and Critical Layers in the Kuroshio Extension from an Eddying Ocean Model. *Journal of Physical Oceanography*, **44 (8)**, 2191–2211, https://doi.org/10.1175/JPO-D-13-0258.1.

Chouksey, A., A. Griesel, M. Chouksey, and C. Eden, 2022: Changes in Global Ocean Circulation due to Isopycnal Diffusion. *Journal of Physical Oceanography*, **52 (9)**, 2219–2235, https://doi.org/10.1175/JPO-D-21-0205.1.

Csanady, G. T., 1976: Topographic Waves in Lake Ontario. *Journal of Physical Oceanography*, **6 (1)**, 93–103, https://doi.org/10.1175/1520-0485(1976)006⟨0093:TWILO⟩2.0.CO;2.

Davis, R. E., 1987: Modeling eddy transport of passive tracers. *Journal of Marine Research*, **45 (3)**, 635–666, https://doi.org/10.1357/002224087788326803.

Davis, R. E., 1991: Observing the general circulation with floats. *Deep Sea Research Part A. Oceanographic Research Papers*, **38**, S531–S571, https://doi.org/10.1016/S0198-0149(12)80023-9.

DelSole, T., 2004: Stochastic models of quasigeostrophic turbulence. *Surveys in Geophysics*, **25 (2)**, 107–149, https://doi.org/10.1023/B:GEOP.0000028164.58516.b2.

Dijkstra, H. A., 2008: *Dynamical Oceanography*. Springer US, https://doi.org/10.1007/978-3-540-76376-5.

Dritschel, D. G., and M. E. McIntyre, 2008: Multiple Jets as PV Staircases: The Phillips Effect and the Resilience of Eddy-Transport Barriers. *Journal of the Atmospheric Sciences*, **65 (3)**, 855–874, https://doi.org/10.1175/2007JAS2227.1.

Eady, E. T., 1949: Long Waves and Cyclone Waves. *Tellus*, **1 (3)**, 33–52, https://doi.org/10.3402/tellusa.v1i3.8507.

Eden, C., 2007: Eddy length scales in the North Atlantic Ocean. *Journal of Geophysical Research*, **112 (C6)**, C06 004, https://doi.org/10.1029/2006JC003901.

669 Eden, C., 2011: A closure for meso-scale eddy fluxes based on linear instability theory. *Ocean*
670 *Modelling*, **39 (3-4)**, 362–369, https://doi.org/10.1016/j.ocemod.2011.05.009.

671 Eden, C., and R. J. Greatbatch, 2008: Towards a mesoscale eddy closure. *Ocean Modelling*, **20 (3)**,
672 223–239, https://doi.org/10.1016/j.ocemod.2007.09.002.

673 Ferrari, R., and M. Nikurashin, 2010: Suppression of eddy diffusivity across jets in the
674 Southern Ocean. *Journal of Physical Oceanography*, **40 (7)**, 1501–1519, https://doi.org/
675 10.1175/2010JPO4278.1.

676 Ferreira, D., J. Marshall, and P. Heimbach, 2005: Estimating Eddy Stresses by Fitting Dynamics
677 to Observations Using a Residual-Mean Ocean Circulation Model and Its Adjoint. *Journal of*
678 *Physical Oceanography*, **35 (10)**, 1891–1910, https://doi.org/10.1175/JPO2785.1.

679 Fox-Kemper, B., R. Ferrari, and R. Hallberg, 2008: Parameterization of Mixed Layer Eddies. Part
680 I: Theory and Diagnosis. *Journal of Physical Oceanography*, **38 (6)**, 1145–1165, https://doi.org/
681 10.1175/2007JPO3792.1.

682 Fox-Kemper, B., and Coauthors, 2019: Challenges and Prospects in Ocean Circulation Models.
683 *Frontiers in Marine Science*, **6**, 65, https://doi.org/10.3389/fmars.2019.00065.

684 Gent, P. R., and J. C. McWilliams, 1990: Isopycnal Mixing in Ocean Circulation Models. *Journal of*
685 *Physical Oceanography*, **20 (1)**, 150–155, https://doi.org/10.1175/1520-0485(1990)020⟨0150:
686 IMIOCM⟩2.0.CO;2.

687 Gent, P. R., J. Willebrand, T. J. McDougall, and J. C. McWilliams, 1995: Parameterizing Eddy-
688 Induced Tracer Transports in Ocean Circulation Models. *Journal of Physical Oceanography*,
689 **25 (4)**, 463–474, https://doi.org/10.1175/1520-0485(1995)025⟨0463:PEITTI⟩2.0.CO;2.

690 Gnanadesikan, A., D. Bianchi, and M.-A. Pradal, 2013: Critical role for mesoscale eddy diffusion
691 in supplying oxygen to hypoxic ocean waters. *Geophysical Research Letters*, **40 (19)**, 5194–5198,
692 https://doi.org/10.1002/grl.50998.

693 Gnanadesikan, A., M.-A. Pradal, and R. Abernathey, 2015: Isopycnal mixing by mesoscale
694 eddies significantly impacts oceanic anthropogenic carbon uptake. *Geophysical Research Letters*,
695 **42 (11)**, 4249–4255, https://doi.org/10.1002/2015GL064100.

Gnanadesikan, A., A. Russell, M.-A. Pradal, and R. Abernathey, 2017: Impact of Lateral Mixing in the Ocean on El Nino in a Suite of Fully Coupled Climate Models. *Journal of Advances in Modeling Earth Systems*, **9 (7)**, 2493–2513, https://doi.org/10.1002/2017MS000917.

Green, J. S. A., 1960: A problem in baroclinic stability. *Quarterly Journal of the Royal Meteorological Society*, **86 (368)**, 237–251, https://doi.org/10.1002/qj.49708636813.

Griesel, A., C. Eden, N. Koopmann, and E. Yulaeva, 2015: Comparing isopycnal eddy diffusivities in the Southern Ocean with predictions from linear theory. *Ocean Modelling*, **94**, 33–45, https://doi.org/10.1016/j.ocemod.2015.08.001.

Griffies, S. M., 1998: The Gent–McWilliams Skew Flux. *Journal of Physical Oceanography*, **28 (5)**, 831–841, https://doi.org/10.1175/1520-0485(1998)028⟨0831:TGMSF⟩2.0.CO;2.

Groeskamp, S., S. M. Griffies, D. Iudicone, R. Marsh, A. J. Nurser, and J. D. Zika, 2019: The water mass transformation framework for ocean physics and biogeochemistry. *Annual Review of Marine Science*, **11**, 271–305, https://doi.org/10.1146/annurev-marine-010318-095421.

Groeskamp, S., J. H. LaCasce, T. J. McDougall, and M. Rogé, 2020: Full-Depth Global Estimates of Ocean Mesoscale Eddy Mixing From Observations and Theory. *Geophysical Research Letters*, **47 (18)**, 1–12, https://doi.org/10.1029/2020GL089425.

Grooms, I., A. J. Majda, and K. S. Smith, 2015: Stochastic superparameterization in a quasigeostrophic model of the Antarctic Circumpolar Current. *Ocean Modelling*, **85**, 1–15, https://doi.org/10.1016/j.ocemod.2014.10.001.

Gruber, N., Z. Lachkar, H. Frenzel, P. Marchesiello, M. Münnich, J. C. McWilliams, T. Nagai, and G.-K. Plattner, 2011: Eddy-induced reduction of biological production in eastern boundary upwelling systems. *Nature Geoscience*, **4 (11)**, 787–792, https://doi.org/10.1038/ngeo1273.

Hallberg, R., 2013: Using a resolution function to regulate parameterizations of oceanic mesoscale eddy effects. *Ocean Modelling*, **72**, 92–103, https://doi.org/10.1016/j.ocemod.2013.08.007.

Hogg, N. G., 2000: Low-frequency variability on the western flanks of the Grand Banks. *Journal of Marine Research*, **58 (4)**, 523–545, https://doi.org/10.1357/002224000321511007.

Holloway, G., 1986: Estimation of oceanic eddy transports from satellite altimetry. *Nature*, **323 (6085)**, 243–244, https://doi.org/10.1038/323243a0.

Holloway, G., and S. S. Kristmannsson, 1984: Stirring and transport of tracer fields by geostrophic turbulence. *Journal of Fluid Mechanics*, **141**, 27–50.

Holmes, R. M., S. Groeskamp, K. D. Stewart, and T. J. McDougall, 2022: Sensitivity of a Coarse-Resolution Global Ocean Model to a Spatially Variable Neutral Diffusivity. *Journal of Advances in Modeling Earth Systems*, **14 (3)**, https://doi.org/10.1029/2021MS002914.

Isachsen, P. E., 2011: Baroclinic instability and eddy tracer transport across sloping bottom topography: How well does a modified Eady model do in primitive equation simulations? *Ocean Modelling*, **39 (1-2)**, 183–199, https://doi.org/10.1016/j.ocemod.2010.09.007.

Isachsen, P. E., and O. A. Nøst, 2012: The air-sea transformation and residual overturning circulation within the Nordic Seas. *Journal of Marine Research*, **70 (1)**, 31–68, https://doi.org/10.1357/002224012800502372.

Jansen, M. F., A. Adcroft, S. Khani, and H. Kong, 2019: Toward an Energetically Consistent, Resolution Aware Parameterization of Ocean Mesoscale Eddies. *Journal of Advances in Modeling Earth Systems*, **11 (8)**, 2844–2860, https://doi.org/10.1029/2019MS001750.

Jansen, M. F., A. J. Adcroft, R. Hallberg, and I. M. Held, 2015: Parameterization of eddy fluxes based on a mesoscale energy budget. *Ocean Modelling*, **92**, 28–41, https://doi.org/10.1016/j.ocemod.2015.05.007.

Jones, C. S., and R. P. Abernathey, 2019: Isopycnal Mixing Controls Deep Ocean Ventilation. *Geophysical Research Letters*, **46 (22)**, 13 144–13 151, https://doi.org/10.1029/2019GL085208.

Juricke, S., S. Danilov, N. Koldunov, M. Oliver, D. V. Sein, D. Sidorenko, and Q. Wang, 2020a: A Kinematic Kinetic Energy Backscatter Parametrization: From Implementation to Global Ocean Simulations. *Journal of Advances in Modeling Earth Systems*, **12 (12)**, https://doi.org/10.1029/2020MS002175.

Juricke, S., S. Danilov, N. Koldunov, M. Oliver, and D. Sidorenko, 2020b: Ocean Kinetic Energy Backscatter Parametrization on Unstructured Grids: Impact on Global Eddy-

Permitting Simulations. *Journal of Advances in Modeling Earth Systems*, **12 (1)**, https://doi.org/10.1029/2019MS001855.

Keffer, T., and G. Holloway, 1988: Estimating Southern Ocean eddy flux of heat and salt from satellite altimetry. *Nature*, **332 (6165)**, 624–626, https://doi.org/10.1038/332624a0.

Khani, S., M. F. Jansen, and A. Adcroft, 2019: Diagnosing Subgrid Mesoscale Eddy Fluxes With and Without Topography. *Journal of Advances in Modeling Earth Systems*, **11 (12)**, 3995–4015, https://doi.org/10.1029/2019MS001721.

Kjellsson, J., and L. Zanna, 2017: The Impact of Horizontal Resolution on Energy Transfers in Global Ocean Models. *Fluids*, **2 (3)**, 45, https://doi.org/10.3390/fluids2030045.

Klocker, A., and R. Abernathey, 2014: Global patterns of mesoscale eddy properties and diffusivities. *Journal of Physical Oceanography*, **44 (3)**, 1030–1046, https://doi.org/10.1175/JPO-D-13-0159.1.

Klocker, A., R. Ferrari, and J. H. LaCasce, 2012: Estimating suppression of eddy mixing by mean flows. *Journal of Physical Oceanography*, **42 (9)**, 1566–1576, https://doi.org/10.1175/JPO-D-11-0205.1.

Kong, H., and M. F. Jansen, 2017: The eddy diffusivity in barotropic β-plane turbulence. *Fluids*, **2 (4)**, https://doi.org/10.3390/fluids2040054.

LaCasce, J., 2008: Statistics from Lagrangian observations. *Progress in Oceanography*, **77 (1)**, 1–29, https://doi.org/10.1016/j.pocean.2008.02.002.

LaCasce, J. H., 2000: Floats and f/H. *Journal of Marine Research*, **58**, 61–95, https://doi.org/10.1357/002224000321511205.

LaCasce, J. H., 2017: The Prevalence of Oceanic Surface Modes. *Geophysical Research Letters*, **44 (21)**, https://doi.org/10.1002/2017GL075430.

LaCasce, J. H., R. Ferrari, J. Marshall, R. Tulloch, D. Balwada, and K. Speer, 2014: Float-Derived Isopycnal Diffusivities in the DIMES Experiment. *Journal of Physical Oceanography*, **44 (2)**, 764–780, https://doi.org/10.1175/JPO-D-13-0175.1.

LaCasce, J. H., and S. Groeskamp, 2020: Baroclinic modes over rough bathymetry and the surface deformation radius. *Journal of Physical Oceanography*, **50 (10)**, 2835–2847, https://doi.org/10.1175/JPO-D-20-0055.1.

LaCasce, J. H., and K. G. Speer, 1999: Lagrangian statistics in unforced barotropic flows. *Journal of Marine Research*, **57**, 245–274.

Larichev, V., and I. Held, 1995: Eddy amplitudes and fluxes in a homogeneous model of fully developed baroclinic instability. *Journal of Physical Oceanography*, **25 (10)**, 2285–2297.

Ledwell, J. R., A. J. Watson, and C. S. Law, 1993: Evidence for slow mixing across the pycnocline from an open-ocean tracer-release experiment. *Nature*, **364 (6439)**, 701–703, https://doi.org/10.1038/364701a0.

Ledwell, J. R., A. J. Watson, and C. S. Law, 1998: Mixing of a tracer in the pycnocline. *Journal of Geophysical Research: Oceans*, **103 (C10)**, 21 499–21 529, https://doi.org/10.1029/98JC01738.

Lee, M.-M., A. J. G. Nurser, A. C. Coward, and B. A. de Cuevas, 2007: Eddy Advective and Diffusive Transports of Heat and Salt in the Southern Ocean. *Journal of Physical Oceanography*, **37 (5)**, 1376–1393, https://doi.org/10.1175/JPO3057.1.

Mak, J., A. Avdis, T. David, H. S. Lee, Y. Na, Y. Wang, and F. E. Yan, 2022a: On Constraining the Mesoscale Eddy Energy Dissipation Time-Scale. *Journal of Advances in Modeling Earth Systems*, **14 (11)**, e2022MS003 223, https://doi.org/10.1029/2022MS003223.

Mak, J., J. R. Maddison, D. P. Marshall, and D. R. Munday, 2018: Implementation of a Geometrically Informed and Energetically Constrained Mesoscale Eddy Parameterization in an Ocean Circulation Model. *Journal of Physical Oceanography*, **48 (10)**, 2363–2382, https://doi.org/10.1175/JPO-D-18-0017.1.

Mak, J., D. Marshall, J. Maddison, and S. Bachman, 2017: Emergent eddy saturation from an energy constrained eddy parameterisation. *Ocean Modelling*, **112**, 125–138, https://doi.org/10.1016/j.ocemod.2017.02.007.

Mak, J., D. P. Marshall, G. Madec, and J. R. Maddison, 2022b: Acute Sensitivity of Global Ocean Circulation and Heat Content to Eddy Energy Dissipation Timescale. *Geophysical Research Letters*, **49 (8)**, e2021GL097 259, https://doi.org/10.1029/2021GL097259.

Marshall, J., E. Shuckburgh, H. Jones, and C. Hill, 2006: Estimates and Implications of Surface Eddy Diffusivity in the Southern Ocean Derived from Tracer Transport. *Journal of Physical Oceanography*, **36**, 1806–1821.

Martínez-Moreno, J., A. M. Hogg, and M. H. England, 2022: Climatology, Seasonality, and Trends of Spatially Coherent Ocean Eddies. *Journal of Geophysical Research: Oceans*, **127 (7)**, https://doi.org/10.1029/2021JC017453.

McDougall, T. J., and P. C. McIntosh, 2001: The Temporal-Residual-Mean Velocity. Part II: Isopycnal Interpretation and the Tracer and Momentum Equations. *Journal of Physical Oceanography*, **31 (5)**, 1222–1246, https://doi.org/10.1175/1520-0485(2001)031⟨1222:TTRMVP⟩2.0.CO;2.

Meredith, M. P., A. C. Naveira Garabato, A. M. Hogg, and R. Farneti, 2012: Sensitivity of the Overturning Circulation in the Southern Ocean to Decadal Changes in Wind Forcing. *Journal of Climate*, **25 (1)**, 99–110, https://doi.org/10.1175/2011JCLI4204.1.

Nakamura, N., and D. Zhu, 2010a: Finite-Amplitude Wave Activity and Diffusive Flux of Potential Vorticity in Eddy–Mean Flow Interaction. *Journal of the Atmospheric Sciences*, **67 (9)**, 2701–2716, https://doi.org/10.1175/2010JAS3432.1.

Nakamura, N., and D. Zhu, 2010b: Formation of Jets through Mixing and Forcing of Potential Vorticity: Analysis and Parameterization of Beta-Plane Turbulence. *Journal of the Atmospheric Sciences*, **67 (9)**, 2717–2733, https://doi.org/10.1175/2009JAS3159.1.

Naveira Garabato, A. C., R. Ferrari, and K. L. Polzin, 2011: Eddy stirring in the Southern Ocean. *Journal of Geophysical Research: Oceans*, **116 (9)**, https://doi.org/10.1029/2010JC006818.

Nummelin, A., 2023a: Parameterizing mesoscale eddy buoyancy transport over sloping topography – data. [Dataset]. NIRD research data archive, URL dx.doi.org/10.11582/2023.00129, https://doi.org/10.11582/2023.00129.

Nummelin, A., 2023b: Parameterizing mesoscale eddy buoyancy transport over sloping topography – model setup. [Software]. Zenodo, URL dx.doi.org/10.5281/zenodo.8227382, https://doi.org/10.5281/zenodo.8227382.

Nummelin, A., and P. E. Isachsen, 2024: Parameterizing mesoscale eddy buoyancy transport over sloping topography. Preprint, accepted for publication in J. Adv. Model. Earth Syst. https://doi.org/10.22541/essoar.168394750.04852652/v2.

Pedlosky, J., 1987: *Geophysical Fluid Dynamics*. Springer, New York.

Pennel, R., and I. Kamenkovich, 2014: On the Factors Controlling the Eddy-Induced Transport in the Antarctic Circumpolar Current. *Journal of Physical Oceanography*, **44 (8)**, 2127–2138, https://doi.org/10.1175/JPO-D-13-0256.1.

Pradal, M.-A., and A. Gnanadesikan, 2014: How does the Redi parameter for mesoscale mixing impact global climate in an Earth System Model? *Journal of Advances in Modeling Earth Systems*, **6 (3)**, 586–601, https://doi.org/10.1002/2013MS000273.

Prandtl, L., 1925: Bericht über Untersuchungen zur ausgebildeten Turbulenz. *Zeitschrift für Angewandte Mathematik und Mechanik*, **5**, 136–139.

Pringle, J. M., 2001: Cross-shelf eddy heat transport in a wind-free coastal ocean undergoing winter time cooling. *Journal of Geophysical Research: Oceans*, **106 (C2)**, 2589–2604, https://doi.org/10.1029/2000JC900148.

Redi, M. H., 1982: Oceanic Isopycnal Mixing by Coordinate Rotation. *Journal of Physical Oceanography*, **12 (10)**, 1154–1158, https://doi.org/10.1175/1520-0485(1982)012⟨1154:OIMBCR⟩2.0.CO;2.

Rhines, P., 1970: Edge-, bottom-, and Rossby waves in a rotating stratified fluid. *Geophysical and Astrophysical Fluid Dynamics*, **1 (3-4)**, 273–302, https://doi.org/10.1080/03091927009365776.

Roach, C. J., D. Balwada, and K. Speer, 2016: Horizontal mixing in the Southern Ocean from Argo float trajectories. *Journal of Geophysical Research: Oceans*, **121 (8)**, 5570–5586, https://doi.org/10.1002/2015JC011440.

Roach, C. J., D. Balwada, and K. Speer, 2018: Global Observations of Horizontal Mixing from Argo Float and Surface Drifter Trajectories. *Journal of Geophysical Research: Oceans*, **123 (7)**, 4560–4575, https://doi.org/10.1029/2018JC013750.

Sallée, J., K. Speer, and S. Rintoul, 2011: Mean-flow and topographic control on surface eddy-mixing in the Southern Ocean. *Journal of Marine Research*, **69 (4)**, 753–777, https://doi.org/10.1357/002224011799849408.

Seland, Ø., and Coauthors, 2020: Overview of the Norwegian Earth System Model (NorESM2) and key climate response of CMIP6 DECK, historical, and scenario simulations. *Geoscientific Model Development*, **13 (12)**, 6165–6200, https://doi.org/10.5194/gmd-13-6165-2020.

Srinivasan, K., and W. R. Young, 2014: Reynolds stress and eddy diffusivity of ss-plane shear flow. *Journal of the Atmospheric Sciences*, **71 (6)**, 2169–2185, https://doi.org/10.1175/JAS-D-13-0246.1.

Stammer, D., 1998: On Eddy Characteristics, Eddy Transports, and Mean Flow Properties. *Journal of Physical Oceanography*, **28 (4)**, 727–739, https://doi.org/10.1175/1520-0485(1998)028⟨0727:OECETA⟩2.0.CO;2.

Stewart, A. L., A. Klocker, and D. Menemenlis, 2018: Circum-Antarctic Shoreward Heat Transport Derived From an Eddy- and Tide-Resolving Simulation. *Geophysical Research Letters*, **45 (2)**, 834–845, https://doi.org/10.1002/2017GL075677.

Stewart, A. L., and A. F. Thompson, 2016: Eddy Generation and Jet Formation via Dense Water Outflows across the Antarctic Continental Slope. *Journal of Physical Oceanography*, **46 (12)**, 3729–3750, https://doi.org/10.1175/JPO-D-16-0145.1.

Stewart, K. D., P. Spence, S. Waterman, J. Le Sommer, J.-M. Molines, J. M. Lilly, and M. H. England, 2015: Anisotropy of eddy variability in the global ocean. *Ocean Modelling*, **95**, 53–65, https://doi.org/10.1016/j.ocemod.2015.09.005.

Straub, D. N., 1994: Dispersive effects of zonally varying topography on quasigeostrophic Rossby waves. *Geophysical and Astrophysical Fluid Dynamics*, **75 (2-4)**, 107–130, https://doi.org/10.1080/03091929408203650.

Taylor, G. I., 1921: Diffusion by Continuous Movements. *Proceedings of the London Mathematical Society*, **20**, 196–211.

Thompson, A. F., 2010: Jet Formation and Evolution in Baroclinic Turbulence with Simple Topography. *Journal of Physical Oceanography*, **40 (2)**, 257–278, https://doi.org/10.1175/2009JPO4218.1.

Tulloch, R., and Coauthors, 2014: Direct Estimate of Lateral Eddy Diffusivity Upstream of Drake Passage. *Journal of Physical Oceanography*, **44 (10)**, 2593–2616, https://doi.org/10.1175/JPO-D-13-0120.1.

Vallis, G. K., and M. E. Maltrud, 1993: Generation of Mean Flows and Jets on a Beta Plane and over Topography. *Journal of Physical Oceanography*, **23**, 1346–1362.

Wang, Y., and A. L. Stewart, 2020: Scalings for eddy buoyancy transfer across continental slopes under retrograde winds. *Ocean Modelling*, **147**, 101 579, https://doi.org/10.1016/j.ocemod.2020.101579.

Wei, H., and Y. Wang, 2021: Full-Depth Scalings for Isopycnal Eddy Mixing Across Continental Slopes Under Upwelling-Favorable Winds. *Journal of Advances in Modeling Earth Systems*, **13 (6)**, 1–40, https://doi.org/10.1029/2021MS002498.

Wei, H., Y. Wang, and J. Mak, 2024: Parameterizing Eddy Buoyancy Fluxes Across Prograde Shelf/Slope Fronts Using a Slope-Aware GEOMETRIC Closure. *Journal of Physical Oceanography*, **54 (2)**, 359–377, https://doi.org/10.1175/JPO-D-23-0152.1.

Wei, H., Y. Wang, A. L. Stewart, and J. Mak, 2022: Scalings for Eddy Buoyancy Fluxes Across Prograde Shelf/Slope Fronts. *Journal of Advances in Modeling Earth Systems*, **14 (12)**, https://doi.org/10.1029/2022MS003229.

Wolfram, P. J., and T. D. Ringler, 2017: Quantifying Residual, Eddy, and Mean Flow Effects on Mixing in an Idealized Circumpolar Current. *Journal of Physical Oceanography*, **47 (8)**, 1897–1920, https://doi.org/10.1175/JPO-D-16-0101.1.

Wortham, C., and C. Wunsch, 2014: A multidimensional spectral description of ocean variability. *Journal of Physical Oceanography*, **44 (3)**, 944–966, https://doi.org/10.1175/JPO-D-13-0113.1.

Wunsch, C., 2010: Toward a midlatitude ocean frequency-wavenumber spectral density and trend determination. *Journal of Physical Oceanography*, **40 (10)**, 2264–2281, https://doi.org/10.1175/2010JPO4376.1.

Xie, J., H. Liu, and P. Lin, 2023: A Multifaceted Isoneutral Eddy Transport Diagnostic Framework and Its Application in the Southern Ocean. *Journal of Advances in Modeling Earth Systems*, **15 (7)**, e2023MS003 728, https://doi.org/10.1029/2023MS003728.

Yankovsky, E., L. Zanna, and K. S. Smith, 2022: Influences of Mesoscale Ocean Eddies on Flow Vertical Structure in a Resolution-Based Model Hierarchy. *Journal of Advances in Modeling Earth Systems*, **14 (11)**, https://doi.org/10.1029/2022MS003203.

Zanna, L., P. Porta Mana, J. Anstey, T. David, and T. Bolton, 2017: Scale-aware deterministic and stochastic parametrizations of eddy-mean flow interaction. *Ocean Modelling*, **111**, 66–80, https://doi.org/10.1016/j.ocemod.2017.01.004.

Zika, J. D., J.-B. Sallée, A. J. S. Meijers, A. C. Naveira-Garabato, A. J. Watson, M.-J. Messias, and B. A. King, 2020: Tracking the spread of a passive tracer through Southern Ocean water masses. *Ocean Science*, **16 (2)**, 323–336, https://doi.org/10.5194/os-16-323-2020.